Acta Pharmaceutica Sinica B 2025;15(4):1938−1955

Chinese Pharmaceutical Association
Institute of Materia Medica, Chinese Academy of Medical Sciences

Acta Pharmaceutica Sinica B

www.elsevier.com/locate/apsb
www.sciencedirect.com

ORIGINAL ARTICLE

CDK1-mediated phosphorylation of USP37 regulates SND1 stability and promotes oncogenesis in colorectal cancer

Liang Wu[a,†], Can Cheng[b,†], Ning Zhao[c,†], Liang Zhu[a], Heng Li[d], Jingwen Liu[e], Yang Wu[a], Xi Chen[a,*], Hanhui Yao[a,*], Lianxin Liu[f,*]

[a]*Department of Gastrointestinal Surgery, the First Affiliated Hospital of USTC, Division of Life Sciences and Medicine, University of Science and Technology of China, Anhui Province Key Laboratory of Hepatopancreatobiliary Surgery, Hefei 230001, China*
[b]*Department of Vascular Surgery, the First Affiliated Hospital of USTC, Division of Life Sciences and Medicine, University of Science and Technology of China, Anhui Province Key Laboratory of Hepatopancreatobiliary Surgery, Hefei 230001, China*
[c]*Department of Surgical Oncology, the First Affiliated Hospital of Xi'an JiaoTong University, Xi'an 710061, China*
[d]*Department of Comprehensive Surgery, Anhui Provincial Cancer Hospital, West District of the First Affiliated Hospital of USTC, Division of Life Sciences and Medicine, University of Science and Technology of China, Hefei 230001, China*
[e]*Health Management Center, the First Affiliated Hospital of USTC, Division of Life Sciences and Medicine, University of Science and Technology of China, Heifei 230001, China*
[f]*Department of Hepatobiliary Surgery, the First Affiliated Hospital of USTC, Division of Life Sciences and Medicine, University of Science and Technology of China, Anhui Province Key Laboratory of Hepatopancreatobiliary Surgery, Anhui Provincial Clinical Research Center for Hepatobiliary Diseases, Hefei 230001, China*

Received 3 October 2024; received in revised form 13 November 2024; accepted 11 December 2024

KEY WORDS

Colorectal cancer;
Oncogenesis;
Phosphorylation;
Deubiquitination;

Abstract Colorectal cancer (CRC) poses a severe global health challenge with high incidence and mortality rates. USP37 has been identified as the bona fide deubiquitinase of SND1, playing a critical role in stabilizing SND1, thereby augmenting its oncogenic potential. The interaction between USP37 and SND1 was confirmed through extensive proteomics, ubiquitinomics, and interactomics, underscoring their synergistic effects on CRC proliferation and metastasis. Additionally, CDK1 has emerged as a pivotal

*Corresponding authors.
E-mail addresses: liulx@ustc.edu.cn (Lianxin Liu), yhanhui@ustc.edu.cn (Hanhui Yao), chenxivascular@yeah.net (Xi Chen).
[†]These authors made equal contributions to this work.
Peer review under the responsibility of Chinese Pharmaceutical Association and Institute of Materia Medica, Chinese Academy of Medical Sciences.

https://doi.org/10.1016/j.apsb.2025.02.014

USP37;
SND1;
CDK1;
Dacarbazine

regulator of USP37, phosphorylating it at threonine 631 rather than serine 628, enhancing its deubiquitinase activity, and consequently stabilizing SND1 to drive CRC malignancy further. Histological analyses of human CRC samples linked the upregulation of CDK1 and USP37 with increased SND1 levels and poor patient prognosis. High-throughput virtual screening and subsequent experimental validation identified Dacarbazine as a pharmacological inhibitor of USP37, and its inhibition disrupted SND1 stability, hindering CRC cell proliferation and metastasis. This study reveals a novel and promising molecular mechanism driving CRC progression through the CDK1−USP37−SND1 axis, highlighting the clinical importance of targeting this pathway to improve patient outcomes.

1. Introduction

Colorectal cancer (CRC) is a common and deadly malignancy, ranking as the third most prevalent cancer and second most lethal cancer worldwide[1]. Despite significant advances in early diagnosis and treatment, the rapid proliferation and invasive metastasis of CRC often results in late-stage diagnosis for many patients, leading to poor prognosis[2]. Therefore, understanding the mechanisms underlying CRC proliferation and invasion and identifying new therapeutic targets is imperative to improve patient survival rates and quality of life.

Deubiquitinating enzymes (DUBs) play pivotal roles in maintaining protein homeostasis[3,4], DNA damage repair[5,6], and cellular stress responses in various biological processes[7]. Specifically, the deubiquitinating enzyme USP37 has been implicated in protein degradation and cell cycle regulation in multiple cancers[8]. Although our previous reports indicated that USP37-mediated deubiquitination of Snail1 promotes the proliferation and migration of gastric cancer cells[9]. While recent studies have linked USP37 to angiogenesis and metastasis through β-catenin stabilization in CRC[10], the comprehensive understanding of USP37's specific role in CRC proliferation and invasive metastasis is incomplete. Thus, further investigation into how *USP37* functions in CRC and its potential as a therapeutic target is crucial.

Nucleic acid nuclease domain protein 1 (SND1), also known as Tudor-SN, p100, or MTDH, is a multifunctional protein involved in many cellular processes[11]. SND1 comprises various structural domains, such as the SN and Tudor domains and nuclear localization signals, indicating its extensive interactions with numerous cellular components. It plays a pivotal role in RNA processing activities such as splicing, editing, and miRNA processing, thereby influencing post-transcriptional gene regulation[11]. In the context of cancer, *SND1* is implicated in mechanisms related to cellular proliferation[12], metastatic spread[13], and drug resistance[14]. In summary, *SND1* has emerged as a crucial factor in the pathophysiology of cancer, with multifaceted roles in cellular functions, cancer progression, and therapy, drawing widespread attention to its potential as a therapeutic target.

A critical aspect of CRC progression is the interplay between post-translational modifications, especially phosphorylation and ubiquitination. Phosphorylation and deubiquitination are pivotal processes that regulate protein stability, function, and activity, maintaining cellular homeostasis[15,16]. Phosphorylation, a reversible modification catalyzed by protein kinases, plays a pivotal role in signaling pathways, cell cycle regulation[17], and DNA repair[18], among other critical cellular processes. Ubiquitination involves the covalent attachment of the small protein ubiquitin to target proteins, impacting protein degradation as well as protein localization, activity, and regulatory interactions. Specifically, the phosphorylation of DUBs can modulate their deubiquitinating activity, thereby regulating the stability of their target proteins[15]. In the context of diseases, particularly cancer, dysregulation between phosphorylation and deubiquitination can lead to epithelial−mesenchymal transition[19] and impaired DNA repair[20], underscoring the importance of this interplay in pathophysiology. Consequently, therapeutic strategies targeting DUBs or the kinases that regulate them are receiving significant attention in oncology.

Cyclin-dependent kinases (CDKs) comprise a large family that is essential for the cell cycle process. Among them, *CDK1* is not only a principal regulator of the cell cycle but also phosphorylates various non-cell cycle proteins that are closely linked to tumor onset and progression[21]. These phosphorylation events affect numerous critical biological processes, including DNA repair[22], transcription regulation[23], DNA replication[24], apoptosis[25], chromatin structure[26], and mitosis[27], with their dysregulation potentially leading to tumorigenesis. Exploring *CDK1*'s role beyond the cell cycle, especially in the phosphorylation of non-cell cycle proteins like DUBs, could reveal new molecular mechanisms driving cancer progression.

In this study, we focused on understanding the interplay between *CDK1*, *USP37*, and *SND1* in CRC, proposing a new regulatory mechanism whereby CDK1 phosphorylates USP37, enhancing its deubiquitinating activity on SND1. Our research confirmed the direct binding between USP37 and SND1 and further unveiled the pivotal role of USP37 in the deubiquitination and stabilization of SND1. The phosphorylation of USP37 at threonine 631 by CDK1 is a critical step in this process, which enhances USP37's activity and further stabilizes SND1, thus promoting CRC progression. This novel mechanism not only provides potential therapeutic targets for CRC but also holds broader significance for the treatment of other malignancies with similar molecular dysregulations.

2. Materials and methods

2.1. Human tumor samples

Forty-two fresh CRC specimens were obtained from patients who underwent surgical resection, with CRC as the primary diagnosis, at the First Affiliated Hospital of the University of Science and Technology of China. By the guidelines approved by the institutional review board, written informed consent was obtained from all patients at the time of enrollment between 2020 and 2022. Two

CRC tissue arrays, HColA180Su14 and HRec-Ade180Sur-05, were purchased from Shanghai OUTDO Biotech Co., Ltd.

The collection and analysis of all tumors was approved by the research ethics committee of the First Affiliated Hospital of USTC (2021-KY-087), and all experiments were conducted in accordance with the Helsinki Declaration of 1975.

2.2. Transient RNAi knockdown

To transiently reduce gene expression, the cells were transfected with siRNA using Lipofectamine 3000 (ThermoFisher Scientific, Waltham, MA, USA). The siRNA sequences used are listed in Supporting Information Table S1.

2.3. Lentiviral vectors and stable cell lines

Lentiviral transduction was used to stably incorporate *USP37* and *SND1* into the genome. Specific epitope-tagged genes were integrated into the Lenti-EFS-puro vector and co-transfected with psPAX2 and pMD2.G into HEK293T cells to produce lentiviral particles, as described in previous studies[28]. Target cells were then treated with lentiviral supernatants passed through a 0.45 mm filter, and puromycin-resistant colonies were selected for subsequent experiments. To create *USP37* deficient cells, gRNAs were crafted using the online CRISPR design platform (http://crispr.mit.edu) and cloned into the LentiCRISPR v2 vector (Addgene, Cambridge, MA, USA). Lipofectamine 3000 was used to facilitate the transfection process, with puromycin resistance to ensure successful integration. Isolation in 96-well plates was used for further purification. Confirmation of gene overexpression and knockout was conducted using Immunoblotting (IB) analysis. The sequences of the shRNAs, sgRNA, and the respective negative controls used are shown in Supporting Information Table S2.

2.4. RNA isolation and quantitative RT-PCR (qRT-PCR)

Cell sample RNA was isolated using Takara Bio's RNAiso Plus (Takara Bio, Shiga, Japan) reagent kit from Shiga, Japan, according to the manufacturer's protocol. The PrimeScript™ RT Reagent Kit (Takara Bio) from the same company was used to generate cDNA, strictly following the manufacturer's recommended procedures. Real-time PCR was performed using Takara Bio SYBR® Premix Ex Taq™ II (Takara Bio). Gene expression was quantified using the $2^{-\Delta\Delta CT}$ technique, and the specific primers used are detailed in Supporting Information Table S3.

2.5. IB and co-immunoprecipitation (co-IP) assay

For IB procedures, cell lysis was achieved using a specialized lysis buffer composed of 50 mmol/L Tris (pH 7.4), 150 mmol/L NaCl, 1% Triton X-100, 1% sodium deoxycholate, and 0.1% SDS, enhanced with a 1× protease and phosphatase inhibitor cocktail (MedChemExpress, MCE, Monmouth Junction, NJ, USA). The lysed cells were sonicated on ice, employing a 20% amplitude for 20 s intervals (alternating between 10 s of sonication and 10 s of rest). Subsequently, the protein concentrations in the lysates were quantified using the Bradford protein assay (ThermoFisher Scientific). The lysates were then subjected to SDS-PAGE. In the co-IP process, targeted antibodies were used to extract proteins from the lysates. The immunoprecipitated proteins were then washed four times using lysis buffer before being subjected to further IB analysis.

2.6. Protein half-life assays

To determine the half-life of specific proteins, cycloheximide (CHX, MCE) inhibition of protein synthesis was employed. Cells were cultured under standard conditions until approximately 70%−80% confluence and then treated with 100 μg/mL CHX. Cell protein samples were collected at designated time points for immunoblotting analysis to monitor the degradation rate of the target protein.

2.7. Immunohistochemistry (IHC)

Antigen retrieval was performed by heating the sections in citrate buffer solution (10 mmol/L sodium citrate, pH 6.0) in a microwave for 20 min. The sections were subsequently washed three times with PBS and treated for 10 min with 3% hydrogen peroxide at room temperature to block endogenous peroxidase activity. After another PBS wash, sections were incubated with 10% normal goat serum for an hour to block non-specific binding. Primary antibodies, as suggested by the manufacturer, were then applied and the sections were incubated overnight at 4 °C. The following day, the appropriate secondary antibodies were applied for 60 min at room temperature, followed by DAB substrate staining until the appearance of a brown color. Finally, the sections were counterstained with hematoxylin and eosin and sealed with neutral resin. Staining intensity (0 = no, 1 = weak, 2 = moderate, 3 = strong) and the percentage of positively stained cells (0 = 0%, 1 ≤ 25%, 2 = 25%−50%, 3 = 50%−75%, 4 ≥ 75%) were used as evaluation metrics. Scores ranged from 0 to 12, calculated by multiplying these two values, with scores ≥6 indicating high expression and scores <6 indicating low expression.

2.8. Proximity ligation assay (PLA)

Adhering to the procedure outlined by Söderberg et al.[29], PLA was performed using an *in situ* PLA kit (#DUO92102, Sigma−Aldrich, St. Louis, MO, USA). Cells were grown in confocal dishes to achieve the necessary density and fixed using 4% formaldehyde for 10 min, followed by three PBS washes. For membrane permeabilization, 0.1% Triton X-100 in PBS was added for 10 min. After permeabilization, the cells were washed with PBS and then subjected to a 1 h block to minimize non-specific interactions. Overnight incubation at 4 °C was done with the primary antibodies. The subsequent day involved an hour of PLA probe incubation and 30 min of exposure to the PLA ligation agent at 37 °C. This was followed by treatment with the PLA amplification reagent for 100 min at 37 °C. A final wash with PBS was conducted before DAPI staining for nuclear visualization. The resulting images were acquired using a Zeiss LSM710 confocal microscope and processed using Zeiss confocal software.

2.9. Statistics and reproducibility

Quantitative analysis was executed utilizing GraphPad Prism 8 (GraphPad Software) or Excel 2013. To determine the statistical relevance between the averages of two or more cohorts, a two-tailed Student's *t*-test or one-way ANOVA was employed. Unless noted in the figure legends, cell cloning formation, and Transwell assays were replicated three times, yielding consistent results. Spearman's rank correlation test was used to analyze the association in IHC data from clinical specimens, while Pearson's correlation analysis was applied to assess the relationship in immunoblot data from fresh clinical samples. The Log-rank test

was used to ascertain the statistical significance of Kaplan−Meier survival plots. Statistical significance was defined as a *P*-value <0.05, indicated as n.s. for not significant. For more detailed information and a summary of the resources used in this work, see the Supporting Information Experimental Procedures.

3. Result

3.1. Specific interaction of USP37, which plays an oncogenic role in CRC tissues, with SND1

In our previous in-depth study of gastric cancer, we noted that the PLAGL2−USP37−Snail1 signaling pathway plays a significant role in the progression of gastric cancer[9]. This discovery piqued our interest in the role of this pathway in other tumors, especially those of the digestive system. Through a thorough analysis of datasets from TCGA, we observed that *USP37* mRNA was significantly overexpressed in CRC tissues (Supporting Information Fig. S1A), but was highly correlated with a better prognosis (Fig. S1B). This preliminary finding prompted us to further investigate the USP37 level, as its function as a deubiquitinating enzyme may play a crucial role in biological processes. We validated this using IHC methods and Kaplan−Meier survival analysis on CRC tissue arrays, discovering that USP37 is highly expressed in CRC and significantly associated with poor prognosis (Fig. 1A and B). In summary, these findings reinforced our hypothesis and led us to select USP37 as an important research target for CRC, further exploring its role in the onset and progression of CRC.

To systematically identify the downstream targets of USP37, we used LC−MS/MS. In our experiments, DLD1 cells were chosen as a model, and transfections were conducted with either USP37 or a vector control. The cells were collected for proteomic and ubiquitinomic LC−MS/MS, as shown in Fig. 1C. Concurrently, we also performed LC−MS/MS analysis of endogenous USP37 interactomics in DLD1 cells. The results revealed interactions between USP37 and various proteins (Supporting Information Tables S4−S6), with SND1 drawing our attention because of its high number of specific peptide segments in USP37 interactomics and its role in malignant tumors (Fig. 1D). To further explore the LC−MS/MS findings for USP37 in CRC, we conducted co-IP experiments to validate the interaction between endogenous USP37 and SND1. The results demonstrated a specific interaction between USP37 and SND1 in SW480 and HCT116 cell lines (Fig. 1E), with similar findings supporting this discovery in DLD1 cell lines (Fig. S1C). To further confirm the interaction between exogenous USP37 and SND1, cells expressing Myc-SND1 and HA-USP37 were co-immunoprecipitated with anti-HA or anti-Myc antibodies. These results unequivocally showed that exogenous USP37 formed a protein complex with exogenous SND1 (Fig. 1F). To elucidate the interaction between USP37 and SND1 and establish its specific subcellular localization, we used immunofluorescence staining to visualize endogenous USP37 and SND1 in the CRC cell lines SW480, HCT116, and DLD1. Detailed colocalization analysis revealed that USP37 and SND1 fluorescence signals overlapped significantly mainly in the nucleus, with a small amount of overlap in the cytoplasm (Fig. 1G, Fig. S1D and S1E). Additionally, similar colocalization experiments in HEK293T cells transfected to express Myc-SND1 and HA-USP37 revealed colocalization mainly in the nucleus (Fig. S1F), suggesting potential interactions between these two proteins in the nucleus, thereby reinforcing the hypothesis that USP37 and SND1 collaboratively participate in certain key biological pathways within the nucleus. Co-IP analysis showed that Myc-SND1 was readily detected in immunoprecipitates of HA-USP37 wild-type (WT) or HA-USP37 Cys350S in HEK293T cells, suggesting that this interaction is not dependent on the DUB enzyme activity of USP37 (Fig. S1G). Next, we sought to determine whether USP37 directly interacted with SND1. PLA validated the direct close *in situ* binding of USP37 and SND1 in SW480 and HCT116 cells (Fig. 1H). GST-pull-down assays also confirmed this conclusion: a direct interaction exists between USP37 and SND1, and the DUB active site of USP37 is not key to their interaction (Fig. 1I). To map the minimal structural domains required for the SND1−USP37 interaction, we generated various truncated mutants of HA-USP37 and Myc-SND1 through two truncation approaches, narrowing down the binding region (Fig. 1J and K, Fig. S1H and S1I). Truncation mutant analysis indicated that the middle sequence of USP37 (340−750 aa) and the SN2 domain of SND1 (166−328 aa) are both necessary and sufficient for their direct interaction (Fig. 1L−N and Fig. S1J−S1M). In summary, our comprehensive analysis elucidated the significant overexpression of *USP37* in CRC, its potential prognostic value, and its specific interaction with SND1.

3.2. USP37 maintains SND1 stability

We confirmed the direct interaction between USP37 and SND1, providing insights into the potential role of USP37 in regulating the stability of SND1. By knocking down the expression of *USP37* in SW480 and HCT116 cell lines, a notable decrease in SND1 levels was observed (Fig. 2A, Supporting Information Fig. S2A and S2B). Moreover, USP37 WT, not its catalytically inactive mutant USP37 Cys350S, upregulated SND1 levels (Fig. 2B and C), and USP37 increased SND1 level in a dose-dependent manner (Fig. 2D and E), indicating that USP37 regulates SND1 in a DUB activity-dependent manner. Ectopic expression of *USP37* significantly upregulated the SND1, which could be partially reversed by expressing *USP37* shRNA (Fig. 2F). However, depletion or overexpression of *USP37* had no significant effect on *SND1* mRNA levels, implying that *USP37* regulates *SND1* at the protein level rather than at the transcriptional level (Fig. 2G and H). We noted that the deletion of *USP37* significantly reduced the SND1 level, which was almost completely reversed by the addition of the proteasome inhibitor MG132 (Fig. 2I and Fig. S2C) or by overexpression of *USP37* plasmids with anti-shRNAs (Fig. 2J), suggesting that *USP37* regulates *SND1* primarily through the proteasome pathway. To demonstrate that USP37 could affect the stability of SND1 itself, we used CHX to block protein synthesis and detected SND1 levels after intervening in USP37 expression. The enhanced expression of *USP37* WT, but not *USP37* Cys350S, significantly increased the stability of SND1 with a prolonged half-life in DLD1 cells (Fig. 2K and Fig. S2D), while knockdown of *USP37* in SW480 and HCT116 cells led to unstable SND1 with a shortened half-life (Fig. 2L and M, Fig. S2E and S2F). Summarizing these results, it is evident that USP37 positively regulates the stability of SND1 through its deubiquitinase activity, involving the proteasome degradation pathway. These findings provide important clues for further research on the role of *USP37* in CRC progression.

3.3. USP37 deubiquitinates SND1

To investigate whether USP37 catalyzes the deubiquitination of SND1, we conducted deubiquitination assays under various

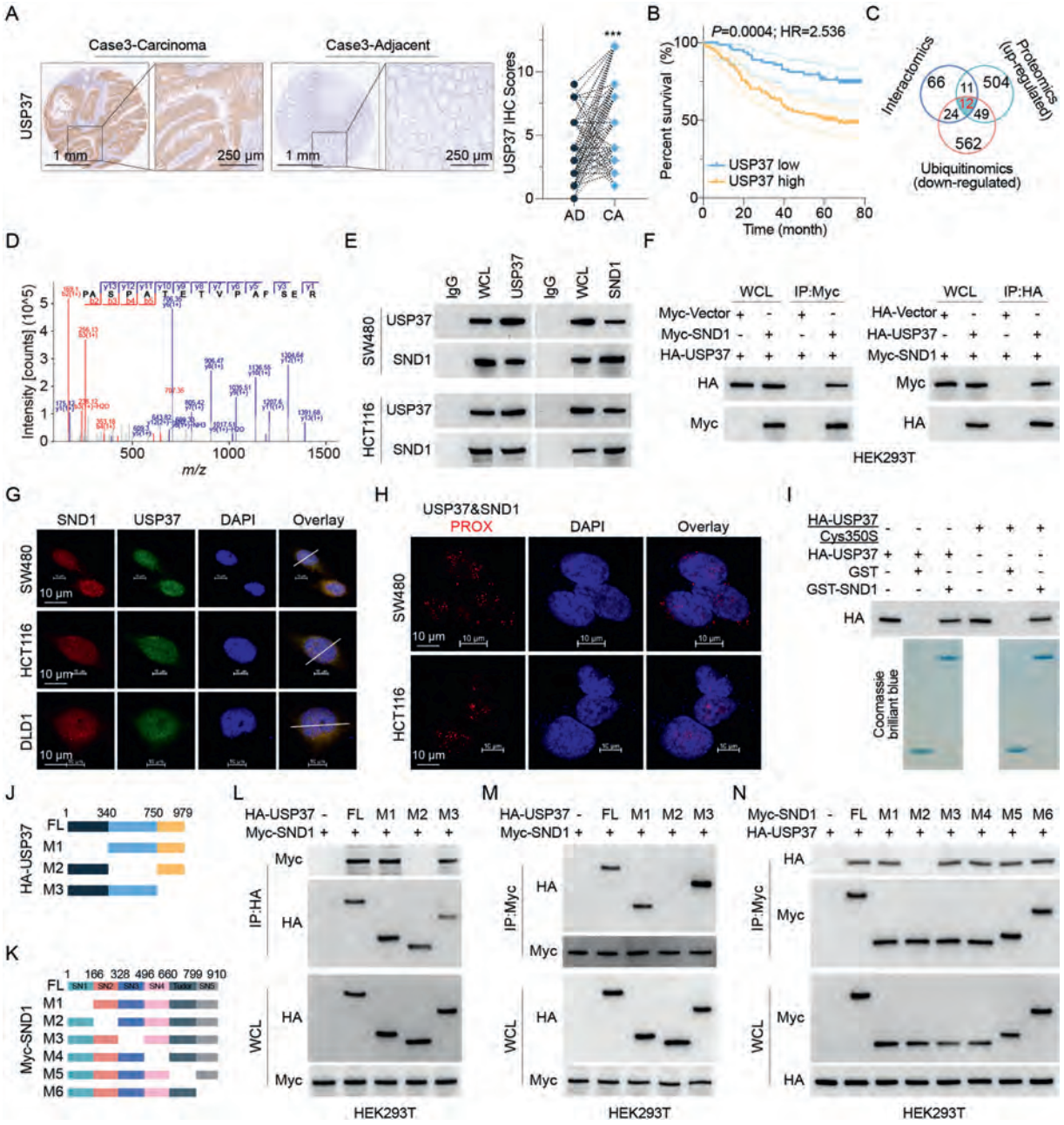

Figure 1 Specific interaction of USP37, which plays an oncogenic role in CRC tissues, with SND1. (A) IHC staining of USP37 was performed on 180 human CRC specimens. Representative consecutive sections from the samples are depicted. Scale is as indicated. The Wilcoxon matched-pairs test was employed to compare cancerous tissues (CA) with matched adjacent tissues (AD). (B) Kaplan−Meier survival curves for CRC patients with high ($n = 115$) and low ($n = 65$) USP37 levels were delineated. (C) A Venn diagram depicts proteins upregulated, ubiquitin-modified proteins downregulated, and USP37 binding proteins in DLD1 cells overexpressing USP37 (USP37 *vs.* vector), as determined by LC−MS/MS. (D) LC−MS/MS analysis of SND1 peptides within USP37 immunoprecipitates was conducted. (E) IP analysis using USP37 and SND1 antibodies was performed on cell lysates from SW480 and HCT116, followed by IB analysis. (F) HEK293T cells were co-transfected with HA-USP37 and Myc-SND1. Cell lysates were then subjected to IP using anti-HA or anti-Myc antibodies. (G) Representative images of fixed SW480, HCT116, and DLD1 cells after immunofluorescent staining with antibodies against USP37 (green) and SND1 (red). Nuclei were counterstained with DAPI (blue). Scale bar, 10 μm. (H) Representative images of *in situ* PLA for USP37/SND1 using anti-USP37 and anti-SND1 antibodies in fixed SW480 and HCT116 cells. The PLA-detected proximity complexes are denoted by fluorescent rolling circle products (red dots). Scale bar, 10 μm. (I) Purified HA-USP37 WT or USP37 Cys350S were incubated with GST or GST-SND1 coupled to glutathione-sepharose beads. HA-tagged proteins retained on sepharose were detected using IB. Recombinant GST-SND1 purified from bacteria was analyzed using SDS-PAGE and Coomassie Brilliant Blue staining. (J, K) Schematic representations of HA-tagged full-length (FL) USP37, Myc-tagged FL SND1, and their various deletion mutants. (L, M) In HEK293T cells, Myc-SND1 and HA-tagged FL USP37 or its deletion mutants were co-transfected and subjected to IP analysis using HA or Myc magnetic beads, followed by IB analysis with Myc and HA antibodies. (N) In HEK293T cells, HA-USP37 and Myc-tagged FL SND1 or its deletion mutants were co-transfected and subjected to IP analysis using Myc magnetic beads, followed by IB analysis with antibodies against HA and Myc.

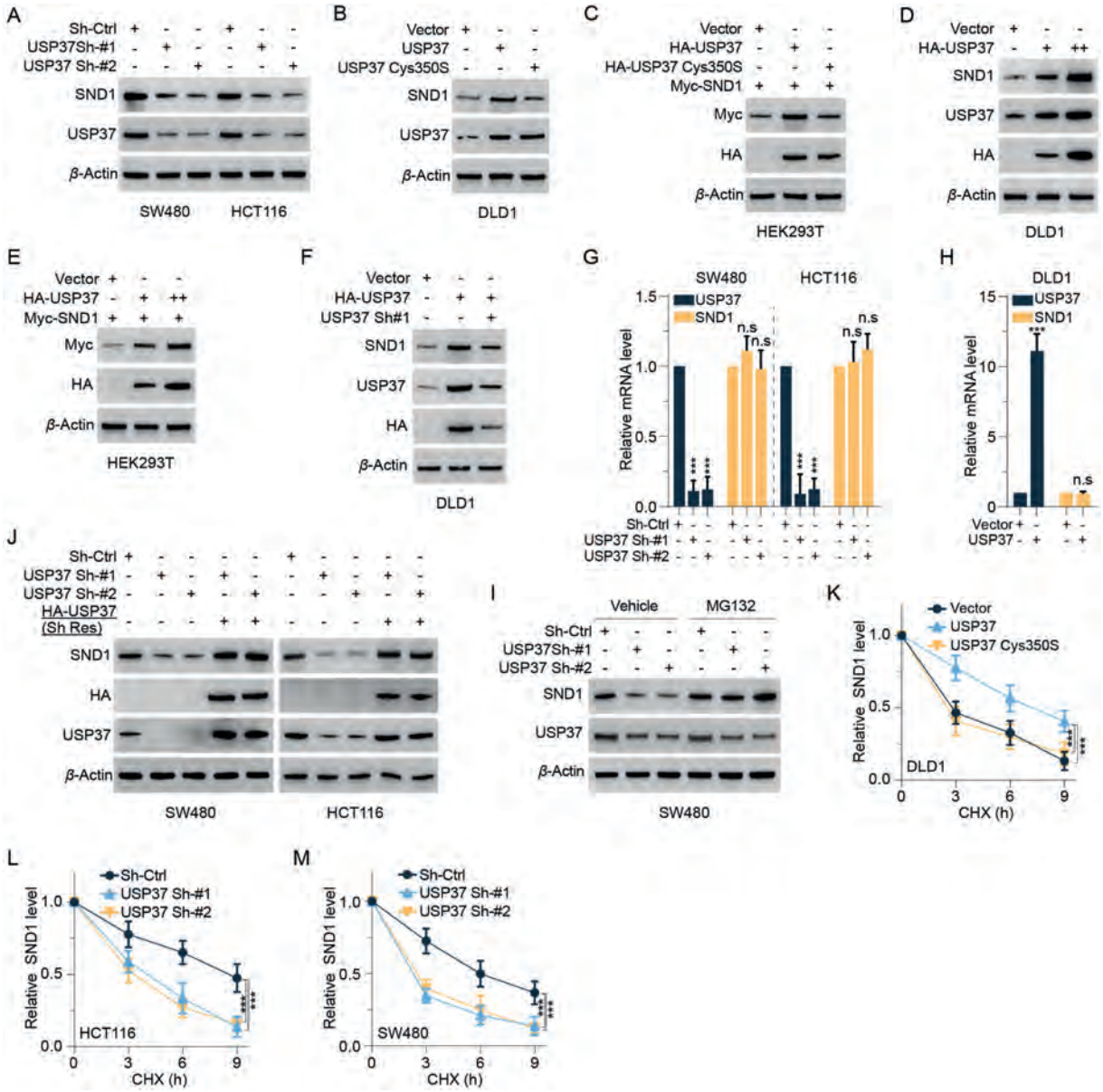

Figure 2 USP37 maintains SND1 stability. (A) USP37 was knocked down in SW480 and HCT116 cells using two independent shRNAs. Subsequently, IB analysis was performed to determine the SND1 level. (B, C) USP37 WT or Cys350S mutant was overexpressed in DLD1 (B) and HEK293T (C) cells. (D, E) Increasing amounts of USP37 were transfected into HEK293T (C) and DLD1 (D) cells, and SND1 level was detected. (F) DLD1 cells were transduced with HA-USP37 WT alone or in combination with *USP37* shRNA, and SND1 levels were analyzed by IB analysis. (G, H) The qRT-PCR analysis was conducted to assess *SND1* mRNA in SW480 and HCT116 cells with depleted endogenous USP37 *via* two independent shRNAs. (I) SW480 cells transfected with two independent *USP37* shRNAs were treated with or without the proteasome inhibitor MG132 (20 μmol/L, 8 h), followed by an analysis of USP37 and SND1. (J) IB analysis of SND1 levels was conducted in SW480 and HCT116 cells transduced with *USP37* shRNA and shRNA-resistant (Sh-Res) HA-USP37. (K) DLD1 cells transfected with USP37 or USP37 Cys350S were treated with 100 μg/mL CHX, harvested at indicated times, and then subjected to IB with antibodies against SND1 and USP37. Quantification of SND1 levels relative to β-actin is shown. (L, M) HCT116 (L) and SW480 (M) cells stably expressing control shRNA (shRNA-Ctrl) or *USP37* shRNA were treated with 100 μg/mL CHX, followed by IB with antibodies against SND1 and USP37. Quantification of SND1 levels relative to β-actin is displayed. (G, H, K, L, and M) Results are quantified and represented as mean ± SD from three independent experiments. ***$P<0.001$ indicates a statistically significant difference, 'ns' indicates no statistical significance, determined by one-way ANOVA (G, K, L, and M) and two-tailed Student's *t*-test (H).

conditions. In HEK293T cells and DLD1, Myc-SND1, and His-Ubi were co-expressed with either USP37 WT or USP37 Cys350S mutant. Following the IP of SND1 from cell lysates treated with MG132, we observed that SND1 was highly ubiquitinated. USP37 WT significantly reduced the ubiquitination level of SND1 in a dose-dependent manner, whereas USP37 Cys350S did not exhibit this effect (Fig. 3A−C). To demonstrate that SND1 is a direct substrate for USP37 deubiquitination, we incubated poly-ubiquitinated SND1 with purified HA-USP37 WT or HA-USP37 Cys350S *in vitro*. We found that purified HA-USP37 WT, but

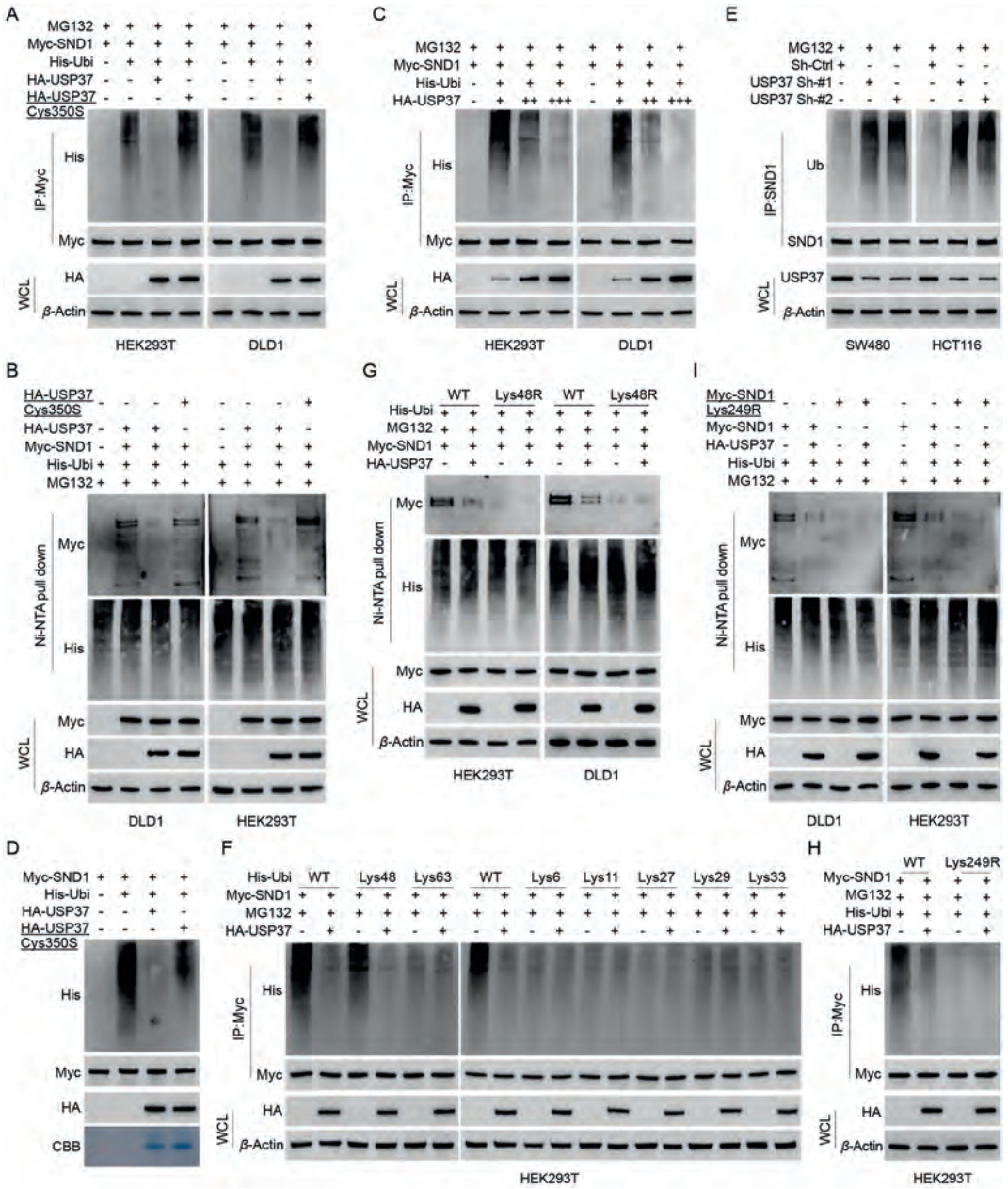

Figure 3 USP37 deubiquitinates SND1. (A) HEK293T or DLD1 cells were co-transfected with Myc-SND1, His-Ubi, and HA-USP37 WT or USP37 Cys350S. Cell lysates were subjected to IP with Myc beads, followed by IB with anti-His and anti-Myc antibodies. Cells were harvested after treatment with 20 μmol/L MG132 for 8 h. (B) Cells co-transfected with the specified plasmids were processed to pull down His-Ubi with Ni-NTA beads, and IB was performed to detect polyubiquitinated SND1. (C) Increasing amounts of USP37 were transfected into HEK293T (C) and DLD1 (D) cells, and treated with MG132 for 8 h before collection. Cell lysates were subjected to IP with Myc beads, followed by IB with anti-His and anti-Myc antibodies. (D) *In vitro* deubiquitination assays were conducted. Ubiquitinated Myc-SND1 was treated with USP37 WT or USP37 Cys350S. Myc-SND1 was immunoprecipitated with Myc beads, followed by IB with anti-HA and anti-His antibodies. Recombinant USP37 WT or USP37 Cys350S was analyzed by SDS-PAGE and Coomassie Brilliant Blue staining. (E) Cells stably expressing shRNA-Ctrl or two independent *USP37* shRNAs were transfected with the described plasmids and treated with MG132 for 8 h. Cell lysates were subjected to IP with SND1 antibody and the ubiquitination of SND1 was detected by IB. (F) HEK293T cells were co-transfected with Myc-SND1, HA-USP37, and His-Ubi WT, Lys6 (specifically Lys6-only), Lys11, Lys27, Lys29, Lys33, Lys48, or Lys63 plasmids to analyze the ubiquitination linkage of SND1. (G) HEK293T cells were co-transfected with Myc-SND1, HA-USP37, and His-Ubi WT or Lys48R (specifically, only Lys48 is mutated to Arg). His-Ubi was pulled down with Ni-NTA beads to analyze the ubiquitination linkage of SND1. (H) HEK293T cells were co-transfected with HA-USP37, His-Ubi, and either Myc-SND1 or Myc-SND1 Lys249R. Cells were collected after treatment with 20 μmol/L MG132 for 8 h. Cell lysates were subjected to IP with Myc beads, followed by IB with anti-His and anti-Myc antibodies. (I) HEK293T and DLD1 cells were co-transfected with the specified plasmids. His-Ubi was pulled down with Ni-NTA beads, and IB was conducted to detect polyubiquitinated Myc-SND1 or Myc-SND1 Lys249R protein.

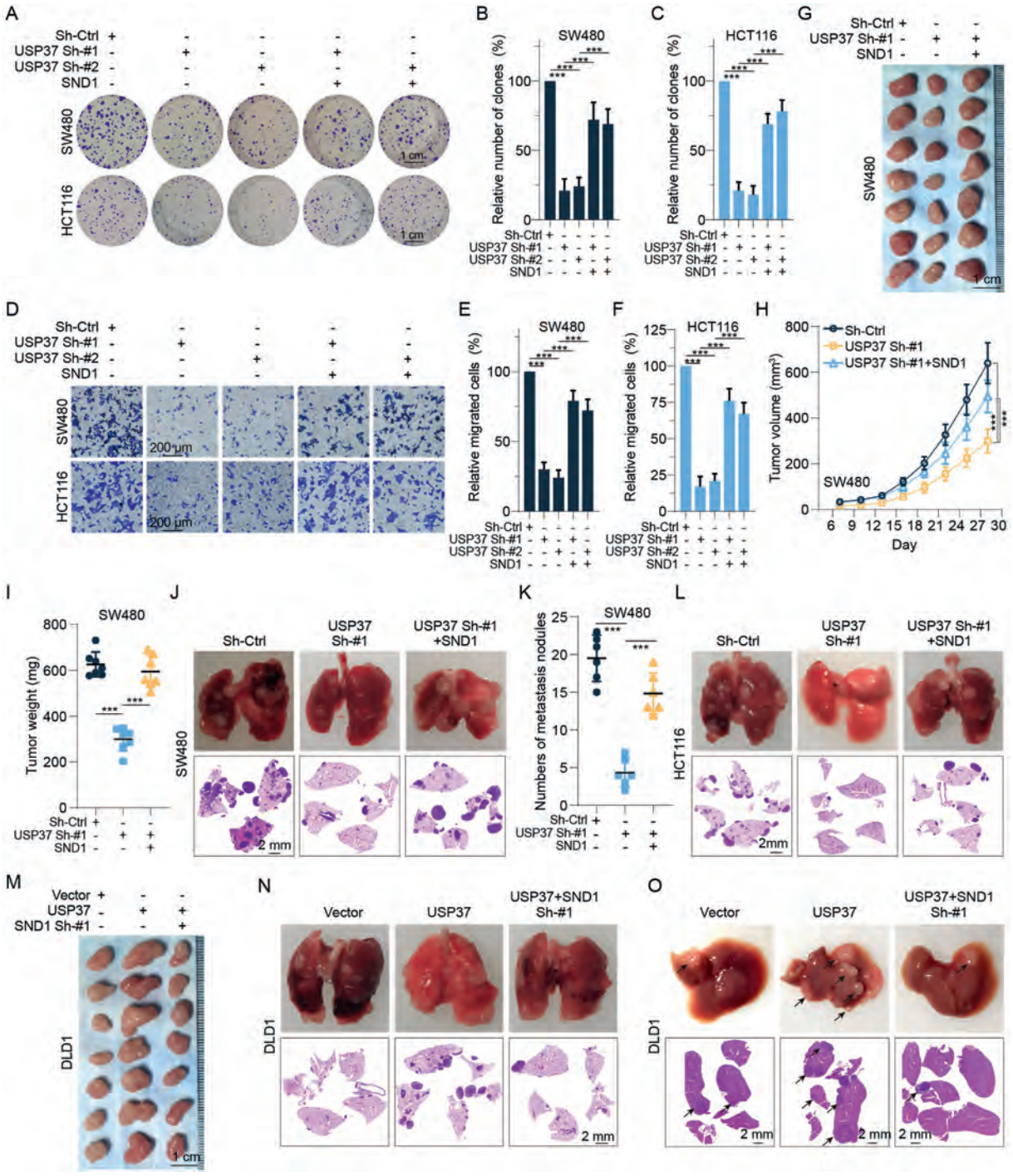

Figure 4 USP37 promotes tumor progression of CRC through stabilizing SND1. (A−F) Cell growth and migration were assessed in SW480 and HCT116 cells transduced with shRNA-Ctrl or *USP37* shRNA, and either vector control or SND1 reconstitution. The number of colonies formed and cells migrated were quantitatively analyzed. Representative images are shown in (A) and (D). Scale bar, 1 cm (A); 200 μm (D). (G−I) Cells as indicated (5×10^6 per mouse) were subcutaneously injected into nude mice ($n = 7$). Tumor volume (H) and weight (I) were calculated. Scale: 1 cm. (J, K) Cells as indicated (2×10^6 per mouse) were injected *via* the tail vein into nude mice to establish a lung metastasis model ($n = 6$). Representative images of lung tissue and H&E-stained sections are presented in (J), along with the calculation of metastatic nodules per group (K). (L) Cells as indicated (2×10^6 per mouse) were injected *via* the tail vein into nude mice to establish a lung metastasis model ($n = 6$). Representative images of lung tissue and H&E-stained sections are presented in (J). (M) SND1 was knocked down in DLD1 cells with overexpression of the *USP37* gene. Cells, as indicated (5×10^6 per mouse), were subcutaneously injected into nude mice to form xenograft tumors ($n = 7$), and gross photographs are shown. (N) Cells as indicated (2×10^6 per mouse) were injected *via* the tail vein into nude mice to establish a lung metastasis model ($n = 6$). Representative images of lung tissue and H&E-stained sections are presented in (N). (O) Cells as indicated (2×10^6 per mouse) were injected beneath the splenic capsule to establish a liver metastasis model ($n = 6$). Representative images of liver tissue and H&E-stained sections are shown in (O). (B, C, E, F, H, I, and K) The results are quantified and represented as mean ± SD. For (B, C, E, and F) $n = 3$ biological replicates. ***P<0.001, one-way ANOVA (B, C, E, F, H, I, and K).

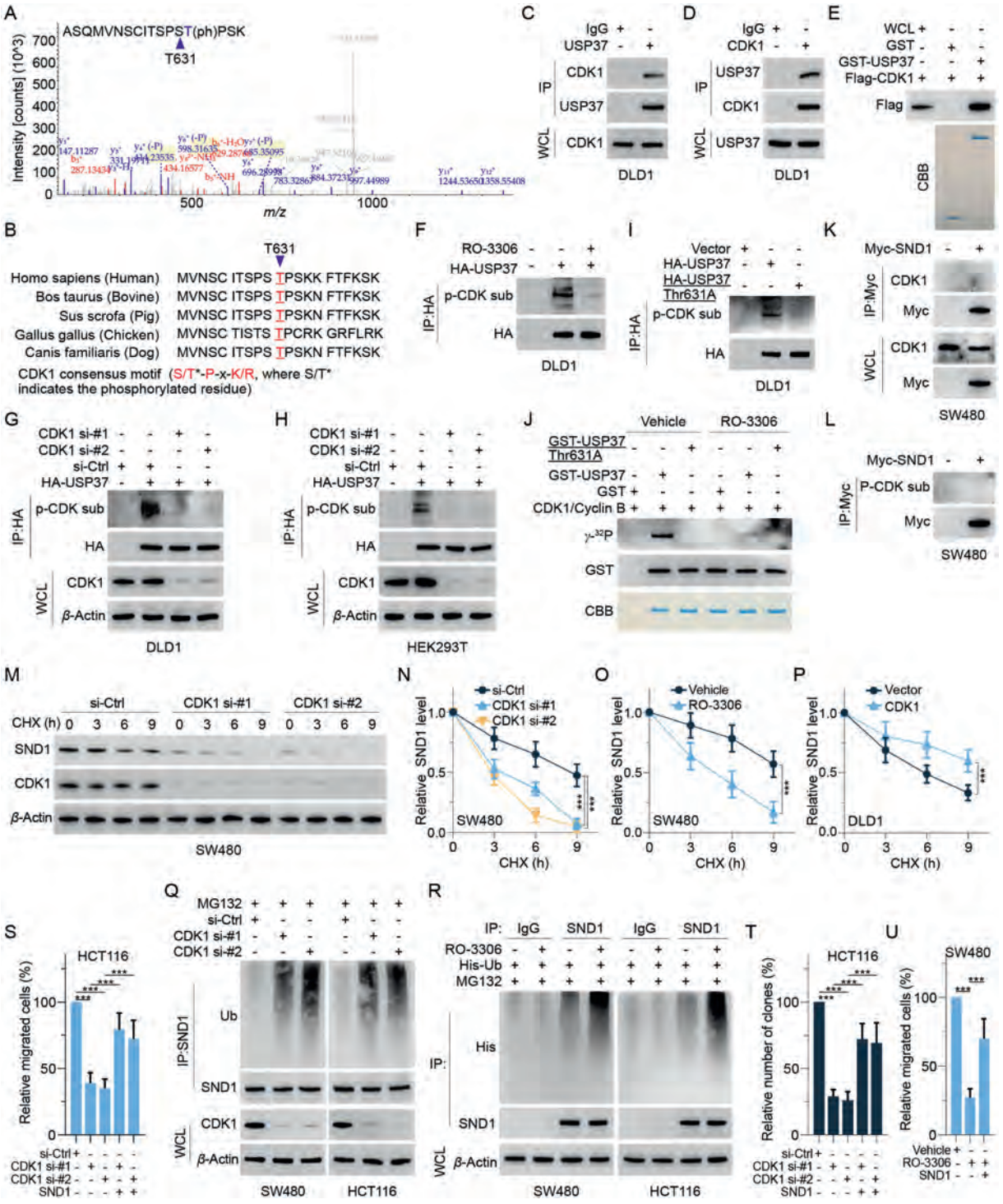

Figure 5 CDK1 binds and phosphorylates USP37. (A) LC−MS/MS identified phosphosite data indicating that the threonine residue corresponding to Thr631 of the USP37 (depicted in blue within the peptide sequence) was phosphorylated. (B) The phosphorylation site at Thr631 of the USP37 is highly conserved throughout evolution. The amino acid sequence of the CDK1-targeted USP37 substrate exhibits conservation across different species. (C, D) IP of DLD1 cell lysates was performed with IgG, anti-USP37 (C), or anti-CDK1 (D) antibodies. The immunoprecipitates were then subjected to IB with designated antibodies. (E) Purified Flag-CDK1 was incubated with GST or GST-USP37 coupled to glutathione-sepharose beads. Proteins retained on the Sepharose were detected by IB with Flag. Recombinant GST-USP37 purified from bacteria was analyzed using SDS-PAGE and Coomassie blue staining. (F) DLD1 cells were transfected with designated plasmids and treated with vehicle or CDK1 inhibitor (RO-3306). IP was performed on cell lysates using an anti-HA antibody, and phosphorylation of USP37 was detected using a phospho-CDK substrate antibody. (G, H) The indicated plasmids and *CDK1* siRNA were transfected into DLD1 and HEK293T cells. IP was performed on cell lysates using an anti-HA antibody, and phosphorylation of USP37 was detected using a phospho-CDK substrate antibody. (I) DLD1 cells were transfected with vector or HA-USP37 (WT or Thr631A mutant). IP was performed on cell lysates using an anti-HA antibody,

not HA-USP37 Cys350S, was capable of interacting with SND1 and specifically disassembling the ubiquitin chains of SND1 *in vitro* (Fig. 3D), indicating that USP37 stabilizes SND1 by directly removing its ubiquitin chains. Consistently, the depletion of *USP37* in SW480 and HCT116 cells significantly increased the ubiquitination level of SND1 (Fig. 3E). These data revealed that USP37-mediated deubiquitination of SND1 is a key mechanism controlling its stability.

Next, we investigated the specificity of USP37 towards the deubiquitination of SND1 in various polyubiquitin chain types. A diverse array of polyubiquitin chain types has been identified, which are formed through isopeptide bonds between different lysine residues, creating unique structures. Lys48 and Lys63 linked ubiquitin chains are the most well-known forms of Ub. Lys48 linked chains are the primary signals for proteasome-dependent protein degradation, meaning that they directly participate in tagging proteins for recognition and breakdown by the proteasome system. In contrast, Lys63 linked chains play a role in many cellular processes, especially those not directly involved in proteasomal degradation mechanisms, such as DNA repair[30,31] and signaling pathways[32]. As for other linkage types, such as those formed by Lys6, Lys11, Lys27, Lys29, and Lys33, the research is not as advanced as that of Lys48 and Lys63. The biological functions and mechanisms of these linkages remain largely unelucidated, and their potential impacts and importance warrant further exploration in future studies. Therefore, we were interested in determining which type of polyubiquitin chain on the SND1 is affected by USP37. As shown in Fig. 3D, USP37 effectively disassembled the Lys48-linked polyubiquitin chains of SND1 but had no significant effect on the non-degradative Lys63 linked and other types of polyubiquitin chains (Fig. 3F and Supporting Information Fig. S3A). To further confirm that USP37 effectively disassembles Lys48-linked polyubiquitin chains of SND1, we used a Lys48-resistant (Lys48R) ubiquitin form for co-transfection. As anticipated, confirmed that Lys48-linked polyubiquitination was crucial for USP37-mediated turnover of SND1 (Fig. 3G and Fig. S3B). Ubiquitinomics following ectopic overexpression of *USP37* revealed that Lys249 may be the primary ubiquitination site of SND1 (Fig. S3C); therefore, we constructed an SND1 Lys249R mutant plasmid for further confirmation. Deubiquitination assays under different conditions proved that the polyubiquitin chains of SND1 that can be specifically removed by USP37 are located at Lys249 (Fig. 3G−I and Fig. S3D). In summary, these results suggest that USP37 is a DUB that plays a crucial role in removing Lys48-linked polyubiquitin chains on the SND1, particularly at the Lys249 residue.

3.4. USP37 promotes tumor progression of CRC through stabilizing SND1

Given the crucial role of SND1 in tumor proliferation, metastasis, and chemotherapy resistance[12-14], we sought to determine whether SND1 is a functional effector of USP37. In DLD1 cells, ectopic expression of *USP37* significantly upregulated the endogenous SND1, enhancing cell proliferation and migration *in vitro*, which could be partially reversed by knocking down SND1 (Supporting Information Fig. S4A−S4G). Conversely, ectopic expression of *SND1* largely rescued the reduced *in vitro* proliferative capacity and invasiveness induced by *USP37* deficiency in HCT116 and SW480 cells (Fig. 4A−F). As *USP37* enhances cancer cell proliferation and invasive metastasis through SND1 *in vitro*, we investigated the function of *USP37 in vivo* proliferation and metastasis of CRC cells *in vivo*. As shown in Fig. 4G, the absence of *USP37* in SW480 cells significantly inhibited the growth of xenograft tumors, as determined by monitoring tumor proliferation curves and weight, whereas reconstruction of SND1 markedly rescued the effects caused by *USP37* deficiency (Fig. 4H and I). Similarly, the absence of *USP37* significantly suppressed lung colonization in SW480 and HCT116 cells, and SND1 reconstruction significantly rescued the effects caused by the loss of *USP37* expression (Fig. 4J−L and Fig. S4H). Additionally, we observed that ectopic overexpression of *USP37* in DLD1 cells notably promoted the growth of xenograft tumors, while knockdown of SND1 significantly rescued the effects caused by *USP37* overexpression (Fig. 4M, Fig. S4I and S4J). The ectopic overexpression of *USP37* in DLD1 cells also markedly promoted lung and liver metastatic colonization, while knocking down SND1 significantly rescued the effects caused by *USP37* overexpression (Fig. 4N and O, Fig. S4K and S4L). In summary, these results revealed a previously unrecognized potential molecular mechanism by which USP37 acts as a deubiquitinating enzyme that promotes CRC cell growth and metastasis, at least partially mediated by its substrate SND1.

3.5. CDK1 binds and phosphorylates USP37

After delving into the deubiquitination of SND1 by USP37, we explored the regulatory mechanisms underlying USP37 activity. Previous studies have shown that phosphorylation plays a key role in regulating the activity of deubiquitinating enzymes[15]. This provided us with a notion that deubiquitinases are not merely effectors regulating the stability of other proteins; their activity is

and phosphorylation of USP37 was detected using a phospho-CDK substrate antibody. (J) *In vitro* kinase assays were conducted with GST-USP37 (WT or Thr631A) affinity-purified from HEK293T cells and cyclin B/CDK1. Coomassie staining of USP37 was used as a loading control. (K) SW480 cells were transfected with vector or Myc-SND1. Cell lysates were subjected to IP using anti-Myc antibody, followed by immunoblotting with designated antibodies. (L) SW480 cells were transfected with vector or Myc-SND1. Cell lysates were subjected to IP using an anti-Myc antibody, and phosphorylation of SND1 was detected using a phospho-CDK substrate antibody. (M, N) A cycloheximide pulse-chase assay was performed in cells, and results were quantified in the right panel (N). The results represent mean ± SD from three independent experiments. (O) SW480 cells were pretreated with RO-3306 (2 μmol/L) for 24 h followed by a cycloheximide pulse-chase assay, and results were quantified. The results are quantified and represented as mean ± SD. from three independent experiments. (P) A cycloheximide pulse-chase assay was performed in cells, and results were quantified. (Q) SW480 and HCT116 cells were transfected with siRNA-Ctrl or two independent CDK1 siRNAs, and IP was performed on cell lysates with anti-SND1 antibodies. IB analysis was conducted to detect the ubiquitination of SND1. (R) Cells were treated with vehicle or RO-3306 for 24 h in the presence of MG-132 (20 μmol/L), and cell lysates were subjected to IP with IgG or anti-SND1, followed by IB to detect the ubiquitination of SND1. (S, T) Cell migration and growth were assessed in SW480 and HCT116 cells transduced with siRNA-Ctrl or CDK1 siRNAs and transfected with vector or SND1. The number of migrated cells (S) and colony formation (T) were quantitatively analyzed. (U) SW480 cells transfected with vector or SND1 were treated with vehicle or RO-3306 for 24 h, and the migration of cells (U) was quantitatively analyzed. (N, O, P, S, T, and U) The results are quantified and represented as mean ± SD. from three independent experiments. ***$P<0.001$, one-way ANOVA (N, S, T, and U), two-tailed Student's *t*-test (O and P).

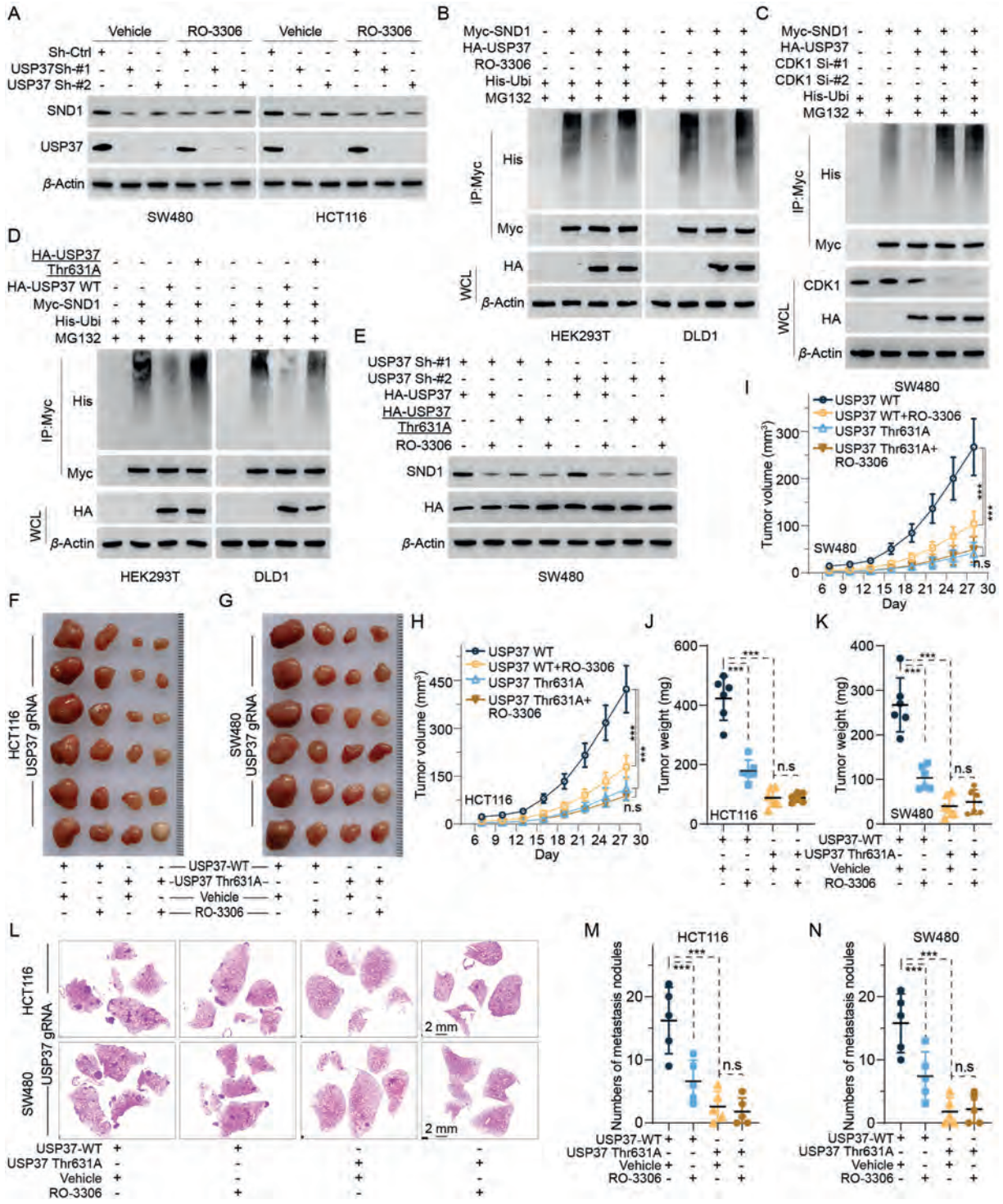

Figure 6 CDK1-mediated phosphorylation activates USP37 towards SND1. (A) USP37 was knocked down in SW480 and HCT116 cells using two independent shRNAs and treated with vehicle or RO-3306. IB analysis was performed to assess the SND1 level. (B) The indicated plasmids were transfected into HEK293T and DLD1 cells, and treated with vehicle or RO-3306. Cell lysates were subjected to IP with an anti-Myc antibody, followed by IB analysis of ubiquitinated SND1. (C) The indicated plasmids and siRNAs were transfected into SW480 cells. IP with anti-SND1 antibody was performed on cell lysates, followed by IB analysis of ubiquitinated SND1. (D) The indicated plasmids were transfected into HEK293T and DLD1 cells. Cell lysates were subjected to IP with an anti-Myc antibody, followed by IB analysis of ubiquitinated SND1. (E) SW480 cells stably expressing *USP37* shRNA were transfected with the specified plasmids, followed by IB analysis of SND1 expression levels. (F, G) HCT116 (F) and SW480 (G) cells with stable knockdown of USP37 were transfected with the indicated plasmids. The cells were then injected into nude mice to form xenograft tumors, with representative gross images shown. Vehicle or RO-3306 treatment was administered at predetermined time points. (H, I) Quantitative analysis of tumor volume for the constructed xenografts from HCT116 (H) and SW480 (I) cells. (J, K) Quantitative analysis of tumor weight for the constructed xenografts from HCT116 (H) and SW480 (I) cells. (L−N) A lung metastasis model

also subject to stringent and complex regulation. Particularly, phosphorylation, a post-translational modification, has been proven to be a crucial regulatory factor in many biological processes. Therefore, we determined the potential phosphorylation sites of USP37 in SW480 cells through LC−MS/MS detection of protein phosphorylation sites, revealing phosphorylation at Thr631, Ser650, Ser652, Ser716, and Ser770 (Fig. 5A and Supporting Information Fig. S5-1). Furthermore, to ascertain which phosphorylation site on USP37 significantly impacts its deubiquitinating activity by targeting SND1, we mutated Thr631, Ser650, Ser652, Ser716, or Ser770 to alanine. The results showed that only USP37 Thr631A exhibited significant suppression of the deubiquitinating activity targeting SND1 compared to USP37 WT (Fig. S5-2A). Concurrently, the strong conservation of Thr631 across multiple species suggests its structural or functional importance (Fig. 5B). We then employed Scansite (https://scansite4.mit.edu) to analyze the potential kinases mediating the phosphorylation of USP37 Thr631, and considering the results of endogenous USP37 interactomics, we preliminarily identified CDK1 as a possible mediator of USP37 Thr631 phosphorylation. To confirm the interaction between endogenous USP37 and CDK1, we conducted co-IP experiments. USP37 was detected in the immunoprecipitates of CDK1 in DLD1 cells (Fig. 5C and D). USP37 was also observed to specifically interact with SND1 in both SW480 and HCT116 cell lines (Fig. S5-2B and S5-2C). To further verify the interaction between exogenous USP37 and CDK1, cells were transfected to express Flag-CDK1 and HA-USP37, followed by co-IP with anti-HA or FLAG antibodies. These results definitively indicate that exogenous USP37 could bind to exogenous CDK1 (Fig. S5-2D and S5-2E). Moreover, purified GST-USP37, but not GST alone, interacted with Flag-CDK1 *in vitro*, demonstrating a direct interaction between USP37 and CDK1 (Fig. 5E).

We further explored whether CDK1 can phosphorylate USP37 and subsequently modulate its tumorigenic role in CRC. As depicted in Fig. 5F, ectopic overexpression of *HA-USP37* in DLD1 cells allowed the detection of phospho-CDK substrates in HA immunoprecipitates; however, pharmacological inhibition of CDK1 with RO-3306 nearly eliminated the detectable phospho-CDK substrates in these immunoprecipitates. Similarly, the knockdown of CDK1 almost completely ablated the detection of phospho-CDK substrates in HA immunoprecipitates (Fig. 5G and H). Previous phosphospecific proteomics results have shown the presence of phosphorylation on Thr631 of USP37, which matches the consensus sequence for CDK substrates. As illustrated in Fig. 5I, phosphorylation of USP37 (USP37 Thr631A) nearly completely abolished the phosphorylation of USP37. Subsequently, we conducted *in vitro* kinase assays in which recombinant CDK1/cyclin B phosphorylated USP37 WT but not USP37 Thr631A (Fig. 5J). In the presence of the CDK1 inhibitor RO-3306, recombinant CDK1/cyclin B-mediated phosphorylation of USP37 WT was also nearly undetectable. CDK2 and CDK1 are important members of the CDK family, playing roles at different stages of the cell cycle, but with some degree of substrate recognition overlap, implying that they might phosphorylate similar or partially overlapping substrate proteins, thus affecting similar cell cycle processes. Dixit et al.[8] reported that CDK2 mediates the phosphorylation of USP37 at Ser628. Hence, we sought to determine whether phosphorylation of USP37 at Ser628 enhances targeting for deubiquitination of SND1 and whether CDK2 could also mediate phosphorylation of USP37 at Thr631. *In vivo* deubiquitination assays and *in vitro* kinase assays indicated that phosphorylation of USP37 at Ser628 had no regulatory effect on targeting SND1 for deubiquitination (Fig. S5-2F), and CDK2-mediated phosphorylation of USP37 at Ser628 did not mediate the phosphorylation of USP37 at Thr631 (Fig. S5-2G and S5-2H). We also tested the possibility that CDK1 acts directly on SND1. As shown in Fig. 5K and L, neither the interaction of CDK1 with SND1 nor the phosphorylation of SND1 was detected. Overall, these results indicated that CDK1 directly interacts with and phosphorylates USP37 rather than SND1.

3.6. CDK1 regulates SND1 stability, CRC cell proliferation, and metastasis

Building on the investigation of the phosphorylation of USP37 by CDK1 and the subsequent stabilization of SND1, this study proposes a new hypothesis that CDK1 may regulate the stability and function of SND1 in CRC. In SW480 and HCT116 cells treated with the CDK1 inhibitor RO-3306 (Fig. S5-2I and S5-2J) or after specific knockdown of *CDK1*, the protein level of SND1 was significantly reduced (Figs. S5-2K); ectopic overexpression of *CDK1* significantly upregulated SND1 level (Fig. S5-2L). However, neither knockdown nor overexpression of *CDK1* affected the mRNA levels of SND1 (Fig. S5-2M and S5-2N). The decrease in SND1 level caused by reduced *CDK1* expression or pharmacological inhibition was reversed by MG132 (Fig. S5-2O and S5-2P). Further analysis revealed that under RO-3306 treatment or CDK1 deficiency, the protein stability of SND1 significantly decreased (Fig. 5M−O, Fig. S5-2Q and S5-2R−U), whereas ectopic overexpression of *CDK1* significantly enhanced the protein stability of SND1, a phenomenon possibly associated with the increased ubiquitination levels of SND1 (Fig. S5-2V and Fig. 5P). To verify this, we examined the *in vivo* ubiquitination levels of SND1 through CDK1 knockdown or pharmacological inhibition and found that SND1 ubiquitination levels significantly increased under RO-3306 treatment or CDK1 knockdown conditions (Fig. 5Q and R). Given these preliminary results, we investigated whether CDK1 regulates the SND1-dependent malignant phenotypes of tumors. Genetic deletion or pharmacological inhibition of *CDK1* expression significantly weakened the proliferative and invasive metastatic abilities of SW480 and HCT116 cells, while the re-expression of *SND1* largely restored these cellular functions (Fig. 5S-2U and S5-2W). Overall, the results of this study revealed a novel cell cycle-independent function of CDK1 in promoting CRC progression by stabilizing SND1, offering a new perspective on the molecular mechanisms of CRC.

3.7. CDK1-mediated phosphorylation activates USP37 towards SND1

Considering that both USP37 and CDK1 enhanced the stability of SND1 and that CDK1 phosphorylated USP37, we hypothesized that the regulation of SND1 by CDK1 might be mediated by the activation of USP37. As shown in Fig. 6A, pharmacological inhibition of CDK1 by RO-3306 significantly reduced the SND1 level in control cells, but did not further decrease the SND1 level

was established using cells from F and G, with the number of metastatic foci quantitatively analyzed (M and N). (H, I, J, K, M, and N) Results are quantified and represented as mean ± SD. ***$P<0.001$, ns indicates no statistical significance, one-way ANOVA (H, I, J, K, M, and N).

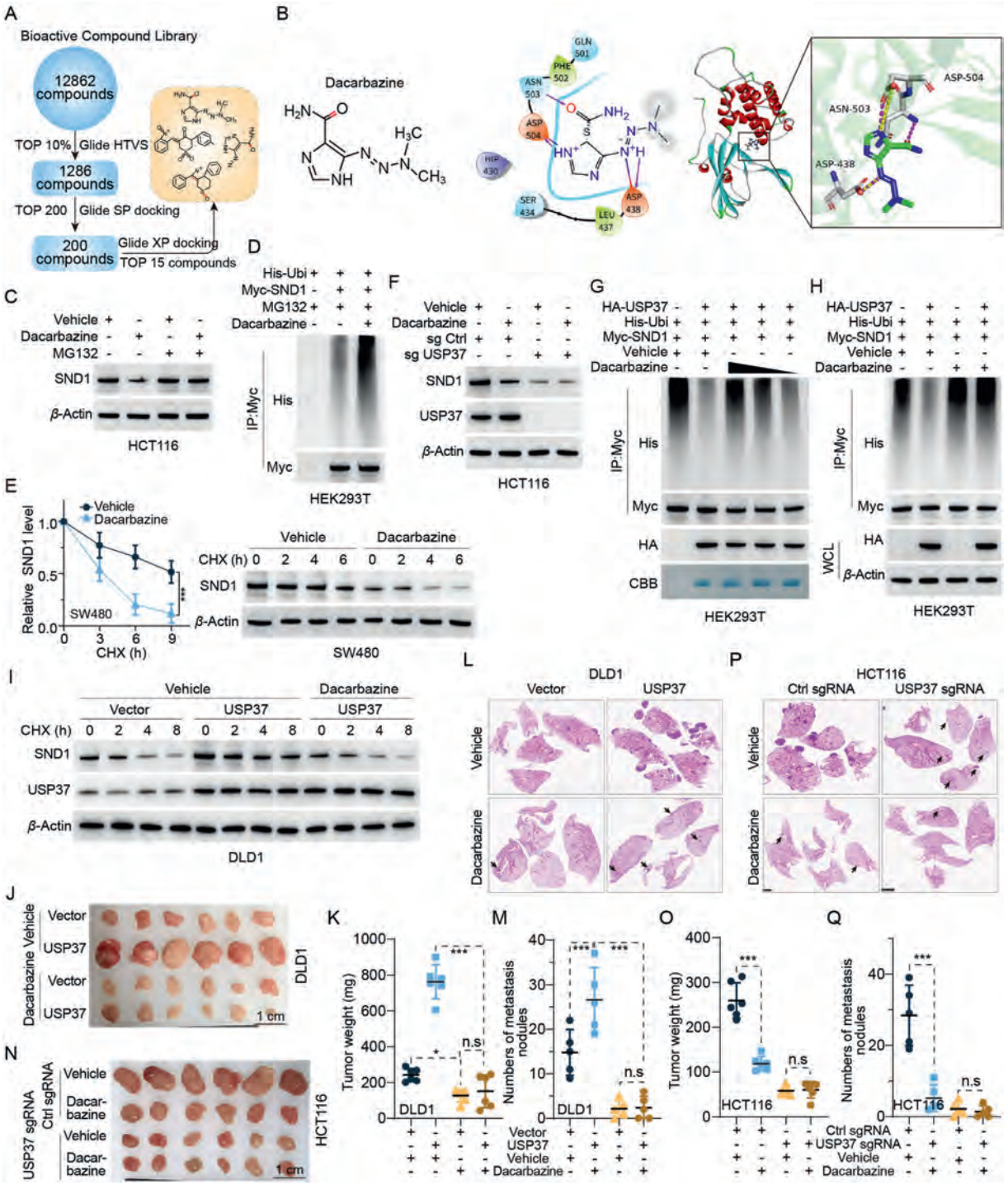

Figure 7 Pharmacological inhibition of USP37 attenuates SND1 stability and inhibits CRC cell proliferation and metastasis. (A) The workflow for HTVS utilized for the identification of USP37 inhibitors. (B) The chemical structure and *in silico* docking of Dacarbazine into the human USP37. (C) IB analysis of SND1 and β-actin in HCT116 cells pretreated with 20 μmol/L MG132 for 1 h, followed by overnight treatment with 15 μmol/L Dacarbazine in the presence of MG132. (D) HEK293T cells co-transfected with Myc-SND1 and His-Ubi, pretreated with 20 μmol/L MG132 for 1 h, then treated overnight with 15 μmol/L Dacarbazine in the presence of MG132. IP was performed using anti-Myc beads, followed by immunoblotting with antibodies against His and SND1. (E) SW480 cells were pretreated with Dacarbazine (15 μmol/L) for 24 h followed by a cycloheximide pulse-chase assay. The results are quantified and represented as mean ± SD from three independent experiments. (F) IB analysis of SND1 expression in control and USP37 gene knockout HCT116 cells treated overnight with 15 μmol/L Dacarbazine. (G) The deubiquitination of SND1 by USP37 at different concentrations of Dacarbazine. HA-USP37 was exposed to 5, 10, and 15 μmol/L Dacarbazine, then incubated with ubiquitinated SND1. The ubiquitination level of SND1 was measured. (H) HEK293T cells co-transfected with Myc-SND1, HA-USP37, and His-Ubi, then treated with 15 μmol/L Dacarbazine for 24 h. After pre-treatment with MG132 (20 μmol/L) for 6 h, IP was performed using anti-Myc beads, followed by IB with antibodies against Myc, HA, and His. (I) DLD1 cells transfected with vector or HA-USP37 were treated with vehicle

in cells lacking *USP37* expression (Fig. 6A). Furthermore, the overexpression of *USP37* significantly reduced the ubiquitination levels of SND1, and this regulation of ubiquitination was blocked by RO-3306 treatment or the absence of CDK1 (Fig. 6B and C). These results indicated that CDK1 is crucial for the enzymatic activity of USP37 on SND1 in CRC. Phosphorylation can regulate interactions between proteins or the enzymatic activity of deubiquitinases. We studied whether the upregulation and malignant progression of SND1 in CRC mediated by CDK1 is mediated by the phosphorylation of USP37. We first investigated whether CDK1 regulates the interaction between USP37 and SND1. As shown in Supporting Information Fig. S6A, the treatment of SW480 cells with RO-3306 did not affect the interaction between USP37 and SND1. Subsequently, we studied whether the phosphorylation of USP37 mediated by CDK1 affects the ubiquitination level of SND1. As depicted in Fig. 6D, overexpression of *USP37 WT* significantly reduced the ubiquitination level of SND1, whereas overexpression of the *USP37 Thr631A* mutant did not. Additionally, we transfected USP37 WT and USP37 Thr631A mutants into SW480 and HCT116 cells with an endogenous USP37 deficiency. We found that the reduction in SND1 level in USP37-deficient cells could be restored by the reconstitution of USP37 WT, but not by the USP37 Thr631A mutant (Fig. S6B), and the reversal effect of USP37 WT on SND1 was similarly blocked by RO-3306 (Fig. 6E and Fig. S7B). Likewise, compared to the USP37 Thr631A mutant, overexpression of *USP37 WT* in SW480 and HCT116 cells significantly prolonged the half-life of SND1 (Fig. S6C and S6D). These results suggested that CDK1-mediated phosphorylation of USP37 is crucial for its deubiquitinase activity on SND1. Next, we studied the function of CDK1-mediated USP37 phosphorylation in SND1-driven malignant processes. We found that compared to the USP37 Thr631A mutant, the reconstitution of USP37 WT in SW480 and HCT116 cells with endogenous USP37 deficiency significantly enhanced the proliferation and invasion-metastasis capability of CRC cells, and the pharmacological inhibition of CDK1 by RO-3306 significantly inhibited these capabilities (Fig. 6F−N and Fig. S6E−S6H). However, in cells reconstituted with USP37 Thr631A mutant, no noticeable effect of RO-3306 was observed (Fig. 6F−N and Fig. S6E−S6H). These results indicated that CDK1-mediated phosphorylation of USP37 is essential for its effect on the SND1-dependent malignant phenotype in CRC progression.

3.8. Pharmacological inhibition of USP37 attenuates SND1 stability and inhibits CRC cell proliferation and metastasis

Our data suggested that targeting USP37 induces enzyme-dependent degradation of SND1, which inspired us to employ USP37 inhibitors to eradicate SND1 for CRC treatment. However, no small-molecule inhibitors of USP37 have been reported to date. Consequently, we conducted high-throughput virtual screening (HTVS) of 12 862 compounds to identify potential USP37 inhibitors (Fig. 7A). Following successive SP and XP docking analyses, the top 20 compounds with the highest docking scores were selected for further validation. In an *in vitro* deubiquitination assay using di-ubiquitin chains as substrates, we observed that USP37 cleaves K48-linked di-ubiquitin, and this cleavage was blocked to varying degrees by most of the 20 preselected compounds, with Dacarbazine exhibiting the strongest inhibition (Supporting Information Fig. S7A and S7B). Protein−ligand interaction fingerprint analysis indicated that Dacarbazine forms hydrogen bonds with Asp438, Asn503, and Asp504 of USP37 and salt bridges with Asp438 and Asp504 (Fig. 7B). Indeed, we sought to determine whether Dacarbazine regulates SND1. Treatment with Dacarbazine downregulated SND1 levels in a dose-dependent manner in SW480 and HCT116 cells (Fig. S7C and S7D), without significantly altering SND1 mRNA levels (Fig. S7E). We further assessed the dependence of Dacarbazine-induced SND1 downregulation on USP37 and the ubiquitin-proteasome system. The proteasome inhibitor MG132 reversed the downregulation of SND1 by Dacarbazine (Fig. 7C and Fig. S7F), suggesting that Dacarbazine promotes SND1 degradation *via* the proteasome. Dacarbazine significantly enhanced SND1 ubiquitination (Fig. 7D and Fig. S7G) and reduced its half-life (Fig. 7E), recapitulating the effects of USP37 gene silencing. Importantly, in HCT116 cells transfected with control sgRNA, Dacarbazine downregulated the SND1, but not in homologous USP37 knockout HCT116 cells (Fig. 7F and Fig. S7H), indicating that the compound destabilizes SND1 through USP37. Dacarbazine effectively inhibits the removal of K48-linked ubiquitin chains at K249 of SND1 (Fig. S7I and S7J). Furthermore, we conducted an *in vitro* de-ubiquitination assay. As shown in Fig. 7G, recombinant USP37 was pretreated with Dacarbazine and co-incubated with ubiquitinated SND1. The results indicated that Dacarbazine significantly disrupted the decline in SND1 ubiquitination induced by USP37, suggesting that the deubiquitinating activity of USP37 was inhibited by Dacarbazine in a concentration-dependent manner. We also evaluated whether Facarbazine effectively blocked the deubiquitinating activity of exogenous USP37, thereby triggering endogenous SND1 degradation. The results showed that Dacarbazine effectively increased the ubiquitination level of SND1 in HEK293T and DLD1 cells (Fig. 7H and Fig. S7K). Treatment with Dacarbazine notably weakened USP37's maintenance of SND1 stability (Fig. S7L and S7M, Fig. 7I). Subsequently, we investigated whether Dacarbazine could also exert sustained pharmacological inhibition of USP37 *in vivo*. The results revealed that the pharmacological inhibition of USP37 by Dacarbazine significantly reduced the proliferation and invasive metastasis of cancer cells (Fig. 7J−M and Fig. S7N). However, no significant

or Dacarbazine (15 μmol/L) for 24 h, then at set time points, CHX (100 μg/mL) was added, and USP37 and SND1 were analyzed by IB. (J, K) DLD1 cells transfected with vector or USP37 were injected into nude mice to form xenograft tumors and are presented in gross photographs. Intraperitoneal injection of Dacarbazine (50 mg/kg) or vehicle was administered at scheduled time points. Quantification of the weight of the xenograft tumors constructed from the cells shown (K). Scale bar, 1 cm. (L, M) A lung metastasis model was constructed using the cells shown in J, and representative images of HE-stained sections are presented. The number of metastatic foci was quantified (M). (N, O) HCT116 cells stably transfected with control or USP37 sgRNA were used to construct xenograft tumors, presented in gross photographs. Intraperitoneal injection of Dacarbazine (50 mg/kg) or vehicle was administered at scheduled time points. Quantification of the weight of the xenograft tumors constructed from the cells shown (O). Scale bar, 1 cm. (P, Q) A lung metastasis model was constructed using the cells shown in N, and representative images of HE-stained sections are presented. The number of metastatic foci was quantified (Q). (E, K, M, O, and Q) The results are quantified and represented as mean ± SD. ***$P < 0.001$, ns indicates no statistical significance, one-way ANOVA (K, M, O, and Q), two-tailed Student's *t*-test (E).

effect of Dacarbazine was observed in homologous USP37 knockout HCT116 cells (Fig. 7N−Q and Fig. S7O). In summary, these data suggest that Dacarbazine holds promise as an effective USP37 inhibitor, inducing SND1 degradation by inhibiting USP37 deubiquitination.

3.9. CDK1, USP37, and SND1 level is upregulated in CRC and positively correlates with poor patient prognosis

To further investigate the clinical relevance of the CDK1−USP37−SND1 axis, we initially analyzed the protein level of CDK1, USP37, and SND1 in 42 pairs of CRC samples *via* IB analysis. We found that in CRC samples, the level of USP37 was positively correlated with SND1 level ($P<0.001$, Pearson $r = 0.5494$) (Fig. 8A and B). Additionally, the level of CDK1 in CRC samples showed a positive correlation with SND1 level ($P<0.001$, Pearson $r = 0.5431$) (Supporting Information Fig. S8A). To further assess the clinical significance of the CDK1−USP37−SND1 axis and determine its correlation in CRC, we performed IHC staining on consecutive sections of colon and rectal cancer tissue microarrays to examine the level of these proteins. IHC results indicated that compared to adjacent or matched neighboring tissues, the levels of CDK1, USP37, and SND1 were significantly upregulated in CRC tissues (Figs. 8C and D, 1A, Fig. S8B−S8D). Moreover, our data also showed that the IHC scores of USP37 and SND1, CDK1 and SND1, as well as CDK1 and USP37, were positively correlated in these tumor samples (Fig. 8E−G). Notably, patients with higher levels of USP37, SND1, or CDK1 in CRC tissues had shorter overall survival than those with lower levels (Figs. 8H and I, and 1B). In summary, these results indicate that these human CRC data align well with our experimental findings regarding the CDK1−USP37 axis-mediated stability of SND1 and the proliferation and invasion-metastasis of CRC cells, and that dysregulation of the CDK1−USP37−SND1 axis leads to poor prognosis in CRC (Fig. 8J).

4. Discussion

Despite recent improvements in screening and treatment techniques for CRC, it remains one of the most common cancers globally, particularly aggressive and lethal in its advanced stages. Proliferation and cancer metastasis are prevalent issues in patients with CRC. Therefore, a deep understanding and overcoming of these challenges, especially in exploring novel therapeutic strategies targeting the mechanisms of proliferation and metastasis, are crucial for enhancing the prognosis of patients with CRC.

In CRC, the upregulation of SND1 has been demonstrated to be a critical factor in promoting cancer cell proliferation and metastasis. However, the structural and functional characteristics of *SND1* present a significant challenge for its direct targeting. Currently, direct strategies for targeting *SND1* are immature. Consequently, exploring strategies that focus on the stability of SND1 or its upstream regulatory mechanisms may provide new therapeutic targets based on *SND1*. In this study, we unveiled the crucial role of the CDK1−USP37 axis in stabilizing SND1 and its oncogenic functions, proposing therapeutic strategies targeting this axis, and potentially offering new insights and treatment approaches to combat CRC proliferation and metastasis. Our experimental results show that, first, by multi-omics LC−MS/MS analysis, USP37 is a bona fide deubiquitinating enzyme of SND1, which directly interacts with and reduces the ubiquitination level of SND1, thus enhancing the stability of SND1. Second, the knockdown of *USP37* expression significantly inhibited cell proliferation and cancer metastasis driven by *SND1* in both *in vitro* cell experiments and *in vivo* animal models. Additionally, we observed that overexpression of *SND1* could partially rescue the phenotypes caused by the loss of *USP37* expression, suggesting that *USP37* exerts its tumor-promoting role in CRC by stabilizing SND1. Moreover, our study highlights a novel regulatory mechanism involving CDK1-mediated phosphorylation of USP37, which stabilizes SND1 and promotes CRC progression. While previous studies have linked *USP37* to various oncogenic processes, our work is the first to identify this specific regulatory axis in CRC, distinguishing it from existing literature and broadening the scope of our understanding of *USP37*'s role in cancer. More importantly, our study also revealed a close correlation between USP37 and SND1 levels in various CRC cell lines and clinical samples. It is also noteworthy that ectopic expression of *SND1* alone could not fully reverse the functional changes caused by the loss of *USP37* in CRC cells, suggesting the potential involvement of other mechanisms regulated by *USP37* in the progression of CRC tumors. Previous studies have shown that *USP37* can regulate the progression of various tumors by controlling the ubiquitination of key proteins such as Snail1[9], BLM[33], HIF2α[34], and c-Myc[35]. This discrepancy might reflect the unique regulatory mechanisms specific to different cancer types or cellular contexts. Therefore, it is necessary for future studies to explore potential substrates of USP37 besides SND1 that might influence CRC metastasis and proliferation to more comprehensively understand its role in cancer progression.

Our research identified *USP37* as a potential therapeutic target for CRC proliferation and metastasis. Thus, elucidating the specific mechanisms underlying the expression or upregulation of *USP37* in CRC is crucial. To date, only a handful of studies have investigated how the expression of *USP37* is induced by various stimuli in different cancer types. For instance, we previously described how *PLAGL2* promotes gastric cancer cell proliferation and invasive metastasis through USP37-mediated deubiquitination of Snail1[9]. Intermittent hypoxia-induced downregulation of microRNA-320b enhances *CDT1* expression through *USP37*, promoting lung cancer tumorigenesis[36]. However, owing to the complexity of signaling pathways, cellular specificity, and potential toxicity issues, the development of direct inhibitors against these signals or other stress conditions poses significant challenges. Therefore, revealing and regulating the activity of USP37 and its downstream target SND1 in CRC may offer a more effective therapeutic approach. However, given Dacarbazine's established role as an antineoplastic agent, we must also consider its potential off-target effects. While our results demonstrate its specificity in inhibiting the deubiquitinating activity of USP37, it is important to acknowledge the possibility of broader cytotoxic effects inherent to Dt effects to ensure the safety and efficacy of targeting *USP37* in a clinical context. By understanding the regulatory mechanisms and networks of *USP37* in CRC, we can lay a solid foundation for developing novel treatment strategies for this complex disease. In this study, we demonstrated that the small-molecule inhibitor Dacarbazine can destabilize SND1 through ubiquitination and proteasomal degradation, indicating that the USP37 deubiquitinase identified here can be inhibited by small molecules. This represents a starting point for targeting USP37, and further development of clinical USP37 inhibitors may require high-throughput chemical screening to identify lead compounds and utilize

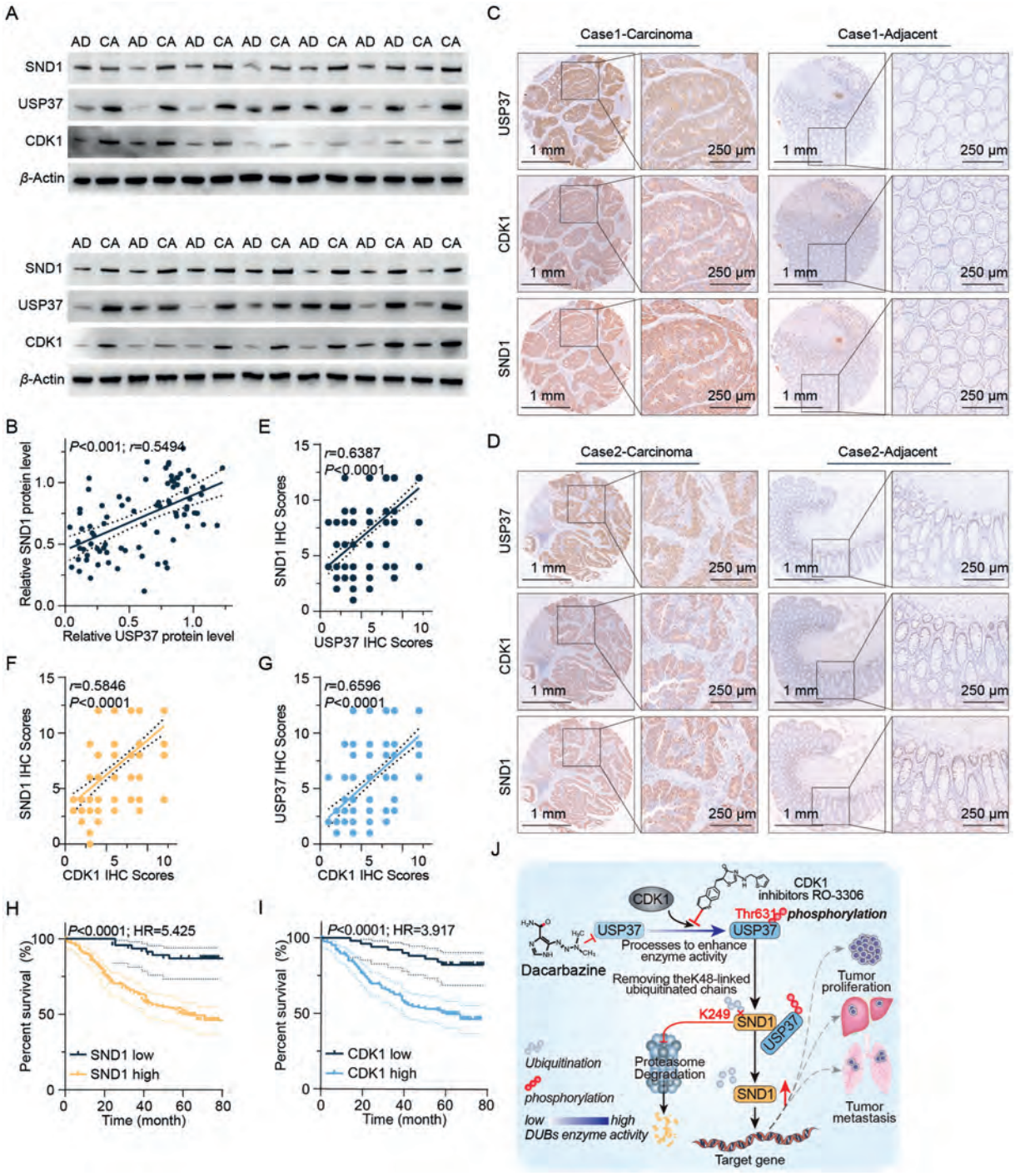

Figure 8 CDK1, USP37, and SND1 expression is upregulated in CRC and positively correlates with poor patient prognosis. (A, B) IB analysis was performed on cell lysates from 42 pairs of CRC tumor tissues and matched adjacent tissues to detect the expression of USP37, SND1, and CDK1. The correlation between USP37 and SND1 in CRC tumor tissues and matched adjacent tissues (B) was analyzed statistically using the chi-square test; Pearson *r* denotes the correlation coefficient. (C, D) Representative images of IHC staining of CDK1, USP37, and SND1 in CRC tumor samples. (E−G) A positive correlation of SND1 expression with USP37 (E) and CDK1 (F) was demonstrated. Additionally, a positive correlation of USP37 expression with CDK1 was shown (G). (H) Kaplan−Meier survival curves for CRC patients with high (n = 132) and low (n = 48) expression of SND1. (I) Kaplan−Meier survival curves for CRC patients with high (n = 127) and low (n = 53) expression of CDK1 protein. (J) The working model illustrates that CDK1-mediated phosphorylation of USP37 regulates SND1 stability and promotes oncogenesis in CRC.

structure−activity relationship analysis to optimize the activity, selectivity, pharmacokinetics, safety, and physical properties of these leads, thereby enabling comprehensive evaluation in animal models.

Phosphorylation is a ubiquitous post-translational modification that plays a critical role in the activity[37], stability[38] and subcellular localization of proteins[39]. Notably, research indicates that the phosphorylation of deubiquitinases is pivotal for their

activity, substrate affinity, and ubiquitin recognition[15]. This prompts our investigation into whether USP37 undergoes phosphorylation by certain protein kinases, and if such post-translational modifications are essential for its tumor-promoting activity. In this study, we demonstrate for the first time the novel function of CDK1 as a direct activator of USP37 in CRC. CDK1, a key regulator of the cell cycle, is aberrantly upregulated in various human malignancies and is associated with tumor staging[40], metastasis[41], and poor prognosis[42]. Our preliminary research revealed that CDK1 activates USP37 and stabilizes SND1 through this pathway to promote *SND1*-driven malignancy, a process independent of other cell cycle phases, indicating the potential clinical significance of targeting the CDK1−USP37−SND1 axis in CRC treatment. We found that CDK1 binds to USP37 and phosphorylates it at Thr631, with the phosphorylation-deficient mutant almost entirely losing its functionality, highlighting the critical nature of these phosphorylation events for USP37 activity targeting SND1. Moreover, in CRC cells, gene silencing or pharmacological inhibition of CDK1 significantly reduces SND1 stability, thereby inhibiting malignant phenotypes driven by SND1. Our findings demonstrate that CDK1-mediated phosphorylation of USP37 is indispensable for its deubiquitinase activity towards SND1- and SND1-driven processes, such as cell proliferation and cancer metastasis (Fig. 8J). Interrupting this phosphorylation event, either by targeting CDK1 or by using a phosphorylation-deficient USP37 mutant, effectively inhibits SND1's stability and function. Thr631, which is located in the UCH domain of USP37, plays a critical role in its functional regulation, suggesting that its phosphorylation could directly affect USP37 substrate recognition and enzymatic activity. Notably, phosphorylation of Thr631 might also induce conformational changes in regions outside the UCH domain of USP37, further affecting its stability and subcellular localization. More importantly, our histological analysis indicated that the upregulation of CDK1, USP37, and SND1 in human CRC specimens correlates strongly with poor patient survival rates, further illustrating the clinical potential of targeting the CDK1−USP37−SND1 axis in CRC treatment. While this study focused on CRC, our findings hold broad significance for understanding and treating other cancers expressing *SND1*, warranting further exploration. Despite the significant findings of this study, there are several limitations that should be acknowledged. First, while we have identified the CDK1−USP37−SND1 axis as a key regulator in CRC, our study primarily focused on cell-based models and *in vivo* animal experiments. Future studies should aim to validate these findings in larger cohorts of human CRC samples to confirm their clinical relevance. Additionally, while Dacarbazine was identified as a specific inhibitor of USP37, further optimization of this compound or the development of more selective USP37 inhibitors is necessary to minimize off-target effects and improve therapeutic efficacy. Moreover, it will be important to explore whether additional substrates of USP37 play a role in CRC progression, as SND1 alone may not fully explain the oncogenic potential of *USP37*. Future studies should also investigate potential compensatory pathways that may be activated when the CDK1−USP37 axis is inhibited.

5. Conclusions

Overall, our study unveils the previously unknown oncogenic role of the CDK1−USP37−SND1 axis in regulating SND1 stability and promoting CRC proliferation and metastasis, affirming its potential clinical value as a therapeutic target in CRC. Notably, the preclinical evidence we provided strongly suggests that targeting the CDK1−USP37 axis can effectively disrupt the stability of SND1, thereby inhibiting cancer cell proliferation and tumor metastasis in CRC. These findings not only deepen our understanding of the molecular mechanisms underlying CRC but also fuel the development of drug discovery and treatment strategies for this prevalent and deadly cancer. By addressing these limitations and continuing to explore the regulatory mechanisms of the CDK1−USP37−SND1 axis, future research can build upon our findings and potentially lead to more effective, targeted therapies for CRC.

Acknowledgments

We extend our sincere appreciation to Mingyang Gao, Shuai Zhou, and Wenxiang Fang for their technical assistance. This research was financially supported by the National Natural Science Foundation of China (Nos. 82103543, 82303235, U19A2008 and 82373232), Fundamental Research Funds for the Central Universities (No. WK9110000159, China), the Natural Science Foundation of Anhui Province (No. 2108085QH340, China), and the China Postdoctoral Science Foundation (No. 2021M693082).

Author contributions

Liang Wu: Writing − original draft, Validation, Methodology, Investigation, Funding acquisition, Data curation. Can Cheng: Methodology, Investigation, Formal analysis, Data curation. Ning Zhao: Methodology, Investigation, Funding acquisition, Formal analysis, Data curation. Liang Zhu: Methodology, Investigation, Formal analysis. Heng Li: Methodology, Investigation. Jingwen Liu: Methodology, Investigation, Data curation. Yang Wu: Methodology, Investigation, Formal analysis, Data curation. Xi Chen: Writing − review & editing, Supervision, Project administration, Methodology, Investigation. Hanhui Yao: Writing − review & editing, Supervision, Project administration, Formal analysis. Lianxin Liu: Writing − review & editing, Supervision, Project administration, Methodology, Formal analysis.

Conflicts of interest

The authors have declared that no conflict of interest exists.

Appendix A. Supporting information

Supporting information to this article can be found online at https://doi.org/10.1016/j.apsb.2025.02.014.

References

1. Morgan E, Arnold M, Gini A, Lorenzoni V, Cabasag CJ, Laversanne M, et al. Global burden of colorectal cancer in 2020 and 2040: incidence and mortality estimates from GLOBOCAN. *Gut* 2023;**72**:338−44.
2. Biller LH, Schrag D. Diagnosis and treatment of metastatic colorectal cancer: a review. *JAMA* 2021;**325**:669−85.
3. Cheng C, Yao H, Li H, Liu J, Liu Z, Wu Y, et al. Blockade of the deubiquitinating enzyme USP48 degrades oncogenic HMGA2 and inhibits colorectal cancer invasion and metastasis. *Acta Pharm Sin B* 2024;**14**:1624−43.
4. Dewson G, Eichhorn PJA, Komander D. Deubiquitinases in cancer. *Nat Rev Cancer* 2023;**23**:842−62.

5. Chen Y, Zhao Y, Yang X, Ren X, Huang S, Gong S, et al. USP44 regulates irradiation-induced DNA double-strand break repair and suppresses tumorigenesis in nasopharyngeal carcinoma. *Nat Commun* 2022;**13**:501.
6. Kim JJ, Lee SY, Hwang Y, Kim S, Chung JM, Park S, et al. USP39 promotes non-homologous end-joining repair by poly(ADP-ribose)-induced liquid demixing. *Nucleic Acids Res* 2021;**49**:11083−102.
7. Niederkorn M, Ishikawa C, K MH, Bartram J, Stepanchick E, J RB, et al. The deubiquitinase USP15 modulates cellular redox and is a therapeutic target in acute myeloid leukemia. *Leukemia* 2022;**36**:438−51.
8. Huang X, Summers MK, Pham V, Lill JR, Liu J, Lee G, et al. Deubiquitinase USP37 is activated by CDK2 to antagonize APC(CDH1) and promote S phase entry. *Mol Cell* 2011;**42**:511−23.
9. Wu L, Zhao N, Zhou Z, Chen J, Han S, Zhang X, et al. PLAGL2 promotes the proliferation and migration of gastric cancer cells *via* USP37-mediated deubiquitination of Snail 1. *Theranostics* 2021;**11**:700−14.
10. Tong D, Yuan J, Wang Z, Yu E, E J. USP37 promotes angiogenesis and metastasis in colorectal cancer by facilitating β-catenin stability. *Am J Cancer Res* 2023;**13**:2323−41.
11. Gutierrez Beltran E, Denisenko TV, Zhivotovsky B, Bozhkov PV. Tudor staphylococcal nuclease: biochemistry and functions. *Cell Death Differ* 2016;**23**:1739−48.
12. Liao SY, Rudoy D, Frank SB, Phan LT, Klezovitch O, Kwan J, et al. SND1 binds to ERG and promotes tumor growth in genetic mouse models of prostate cancer. *Nat Commun* 2023;**14**:7435.
13. Yu L, Liu X, Cui K, Di Y, Xin L, Sun X, et al. SND1 acts downstream of TGFβ1 and upstream of Smurf1 to promote breast cancer metastasis. *Cancer Res* 2015;**75**:1275−86.
14. Chen L, Song Y, Hou T, Li X, Cheng L, Li Y, et al. Circ_0004087 interaction with SND1 promotes docetaxel resistance in prostate cancer by boosting the mitosis error correction mechanism. *J Exp Clin Cancer Res* 2022;**41**:194.
15. Mevissen TET, Komander D. Mechanisms of deubiquitinase specificity and regulation. *Annu Rev Biochem* 2017;**86**:159−92.
16. Zheng N, Shabek N. Ubiquitin ligases: structure, function, and regulation. *Annu Rev Biochem* 2017;**86**:129−57.
17. Nilsson J. Protein phosphatases in the regulation of mitosis. *J Cell Biol* 2019;**218**:395−409.
18. Kciuk M, Gielecinska A, Mujwar S, Mojzych M, Kontek R. Cyclin-dependent kinases in DNA damage response. *Biochim Biophys Acta Rev Cancer* 2022;**1877**:188716.
19. Guan T, Li M, Song Y, Chen J, Tang J, Zhang C, et al. Phosphorylation of USP29 by CDK1 governs TWIST1 stability and oncogenic functions. *Adv Sci* 2023;**10**:e2205873.
20. Sharma A, Alswillah T, Kapoor I, Debjani P, Willard B, Summers MK, et al. USP14 is a deubiquitinase for Ku70 and critical determinant of non-homologous end-joining repair in autophagy and PTEN-deficient cells. *Nucleic Acids Res* 2020;**48**:736−47.
21. Malumbres M, Barbacid M. Cell cycle, CDKs and cancer: a changing paradigm. *Nat Rev Cancer* 2009;**9**:153−66.
22. Chen X, Niu H, Yu Y, Wang J, Zhu S, Zhou J, et al. Enrichment of Cdk1-cyclins at DNA double-strand breaks stimulates Fun30 phosphorylation and DNA end resection. *Nucleic Acids Res* 2016;**44**:2742−53.
23. Aregger M, Kaskar A, Varshney D, Fernandez Sanchez ME, Inesta Vaquera FA, Weidlich S, et al. CDK1−Cyclin B1 activates RNMT, coordinating mRNA Cap methylation with G1 phase transcription. *Mol Cell* 2016;**61**:734−46.
24. Lemmens B, Hegarat N, Akopyan K, Sala Gaston J, Bartek J, Hochegger H, et al. DNA replication determines timing of mitosis by restricting CDK1 and PLK1 activation. *Mol Cell* 2018;**71**:117−28.e3.
25. Zhao Y, Khanal P, Savage P, She YM, Cyr TD, Yang X. YAP-induced resistance of cancer cells to antitubulin drugs is modulated by a Hippo-independent pathway. *Cancer Res* 2014;**74**:4493−503.
26. Schmidt AK, Pudelko K, Boekenkamp JE, Berger K, Kschischo M, Bastians H. The p53/p73-p21(CIP1) tumor suppressor axis guards against chromosomal instability by restraining CDK1 in human cancer cells. *Oncogene* 2021;**40**:436−51.
27. Dietachmayr M, Rathakrishnan A, Karpiuk O, von Zweydorf F, Engleitner T, Fernandez Saiz V, et al. Antagonistic activities of CDC14B and CDK1 on USP9X regulate WT1-dependent mitotic transcription and survival. *Nat Commun* 2020;**11**:1268.
28. Zhang C, Shen L, Zhu Y, Xu R, Deng Z, Liu X, et al. KDM6A promotes imatinib resistance through YY1-mediated transcriptional upregulation of TRKA independently of its demethylase activity in chronic myelogenous leukemia. *Theranostics* 2021;**11**:2691−705.
29. Söderberg O, Gullberg M, Jarvius M, Ridderstrale K, Leuchowius KJ, Jarvius J, et al. Direct observation of individual endogenous protein complexes *in situ* by proximity ligation. *Nat Methods* 2006;**3**: 995−1000.
30. Qin C, Wang YL, Zhou JY, Shi J, Zhao WW, Zhu YX, et al. RAP80 phase separation at DNA double-strand break promotes BRCA1 recruitment. *Nucleic Acids Res* 2023;**51**:9733−47.
31. Vamisetti GB, Saha A, Huang YJ, Vanjari R, Mann G, Gutbrod J, et al. Selective macrocyclic peptide modulators of Lys63-linked ubiquitin chains disrupt DNA damage repair. *Nat Commun* 2022;**13**:6174.
32. Cohen P, Strickson S. The role of hybrid ubiquitin chains in the MyD88 and other innate immune signalling pathways. *Cell Death Differ* 2017;**24**:1153−9.
33. Wu C, Chang Y, Chen J, Su Y, Li L, Chen Y, et al. USP37 regulates DNA damage response through stabilizing and deubiquitinating BLM. *Nucleic Acids Res* 2021;**49**:11224−40.
34. Hong K, Hu L, Liu X, Simon JM, Ptacek TS, Zheng X, et al. USP37 promotes deubiquitination of HIF2α in kidney cancer. *Proc Natl Acad Sci U S A* 2020;**117**:13023−32.
35. Pan J, Deng Q, Jiang C, Wang X, Niu T, Li H, et al. USP37 directly deubiquitinates and stabilizes c-Myc in lung cancer. *Oncogene* 2015; **34**:3957−67.
36. Li W, Huang K, Wen F, Cui G, Guo H, He Z, et al. Intermittent hypoxia-induced downregulation of microRNA-320b promotes lung cancer tumorigenesis by increasing CDT1 *via* USP37. *Mol Ther Nucleic Acids* 2021;**24**:528−41.
37. Cullati SN, Chaikuad A, Chen JS, Gebel J, Tesmer L, Zhubi R, et al. Kinase domain autophosphorylation rewires the activity and substrate specificity of CK1 enzymes. *Mol Cell* 2022;**82**:2006−20.e8.
38. Tu Z, Wang C, Davis AK, Hu M, Zhao C, Xin M, et al. The chromatin remodeler CHD8 governs hematopoietic stem/progenitor survival by regulating ATM-mediated P53 protein stability. *Blood* 2021;**138**: 221−33.
39. Xu D, Wang Z, Xia Y, Shao F, Xia W, Wei Y, et al. The gluconeogenic enzyme PCK1 phosphorylates INSIG1/2 for lipogenesis. *Nature* 2020; **580**:530−5.
40. Chen S, Chen X, Xiu YL, Sun KX, Zhao Y. MicroRNA-490-3P targets CDK1 and inhibits ovarian epithelial carcinoma tumorigenesis and progression. *Cancer Lett* 2015;**362**:122−30.
41. Zhou W, Feng Y, Lin C, Chao CK, He Z, Zhao S, et al. Yin Yang 1-induced long noncoding RNA DUXAP9 drives the progression of oral squamous cell carcinoma by blocking CDK1-mediated EZH2 degradation. *Adv Sci* 2023;**10**:e2207549.
42. Liu X, Wu H, Liu Z. An integrative human pan-cancer analysis of cyclin-dependent kinase 1 (CDK1). *Cancers (Basel)* 2022;**14**:2658.